NTNU – Trondheim
Norwegian University of
Science and Technology

Nonlinear Wave Loads on Offshore Wind Turbines in Storm Condition

Asgeir Hovdelien Midthaug

Marine Technology
Submission date: June 2014
Supervisor: Jørgen Amdahl, IMT
Co-supervisor: Jørgen Ranum Krokstad, IMT

Norwegian University of Science and Technology
Department of Marine Technology

NTNU Trondheim
Norwegian University of Science and Technology
Department of Marine Technology

MASTER THESIS, SPRING 2014

for

Stud.tech. Asgeir Hovdelien Midthaug

Nonlinear Wave Loads on Offshore Wind Turbines in Storm Condition

The background for this thesis is related to the development of offshore wind turbine parks at Dogger Bank outside of England. Good wind conditions and shallow water depth makes this a well suited site for offshore wind industry. One of the main challenges for the industry is to drive down cost without compromising on safety. Design loads are of high importance for the total cost and a balanced approach towards a sufficient conservatism is strived for. Calculations of extreme loads are not well established in the industry, in particular for very dynamic offshore wind turbines in shallow water.

The master thesis will focus on the available tools, models and theories for such computations. Its aim is to investigate the relevance of nonlinear wave loads on the turbine. The work should be carried out in the following steps:

1. A review of present wind turbine analysis procedures is given, and used as a motivation for the thesis.

2. The theory of nonlinear load effects is summarized. A basis for different wave-load models is given, with particular emphasis on the FNV and Rainey model.

3. The wave models are implemented in National Renewable Energy Laboratory's (NREL) open source wind turbine analysis tool FAST.

4. A comparison between linear loads and the nonlinear load models is given for simple dynamic simulations.

5. The influence of vertical modal shape distribution from soil and tower is examined using FAST with a 5MW reference turbine model offered by NREL.

Additional analyses might also show to be of interest during the work.

The work may show to be more extensive than anticipated. Some topics may therefore be left out after discussion with the supervisor without any negative influence on the grading.

The candidate should in her/his report give a personal contribution to the solution of the problem formulated in this text. All assumptions and conclusions must be supported by mathematical models and/or references to physical effects in a logical manner. The candidate should apply all available sources to find relevant literature and information on the actual problem.

The report should be well organised and give a clear presentation of the work and all conclusions. It is important that the text is well written and that tables and figures are used to support the verbal presentation. The report should be complete, but still as short as possible.

The final report must contain this text, an acknowledgement, summary, main body, conclusions and suggestions for further work, symbol list, references and appendices. All figures, tables and equations must be identified by numbers. References should be given by author name and year in the text, and presented alphabetically by name in the reference list. The report must be submitted in two copies unless otherwise has been agreed with the supervisor.

From the report it should be possible to identify the work carried out by the candidate and what has been found in the available literature. It is important to give references to the original source for theories and experimental results. The report should be delivered according to instructions from the faculty, and - if needed – additional material (binder, VD/CD/memory stick) should be delivered to the supervisor.

Deadline: 10 June 2014

Jørgen R. Krokstad
Supervisor

Abstract

Structural ringing can be caused by nonlinear hydrodynamic loads in steep waves, by wave slamming, or by breaking waves. This thesis deals with the first category: nonlinear wave loads on bottom-fixed offshore wind turbines in storm condition. Two higher order forcing models are investigated. The FNV (Faltinsen, Newman, Vinje) model accounts for wave loads on a surface piercing column of up to third order of the incident wave field. It is derived by a perturbation of the non-dimensional wave steepness $kA \ll 1$, and requires the column radius to be of the same order of magnitude as the wave amplitude: $\mathcal{O}(ka) = \mathcal{O}(kA)$. The higher order FNV forces have their maximum at the free surface, and are decaying exponentially with the water depth. Rainey's slender body forces are not derived using a perturbation approach, but rather by conservation of energy principles. It will be shown that there is agreement between the first and second order forces from FNV and Rainey for regular waves in deep water, while the third order component deviates. Both force models are derived in this thesis.

A popular software for dynamic analysis of wind turbines is the open source FAST (Fatigue, Aerodynamics, Structures and Turbulence) code from NREL (National Renewable Energy Laboratory). FAST is capable of producing a time marching simulation of an offshore wind turbine subjected to various environmental loads. However, FAST only supports linear hydrodynamic loads natively. Thus, the force models of interest have to be implemented in the code. An explanation of the theoretical foundation and architecture of FAST is given, as well as details of the force model implementation. A test case in regular waves comparing the individual force components is conducted, where agreement between the first and second order components was shown, as previously stated.

Dynamic analysis of a wind turbine model based on the NREL reference turbine is performed for different environmental condition, operational states and turbine configurations. The first natural frequency of the tower is held fixed for all the configurations, to not coincide with the rotor and blade passing frequencies. The magnitude of the top displacement of the turbine was shown to be relatively independent of different tower configurations and forcing models near the natural frequency. No instances of significant structural response due to higher order effects was observed. The effect was however higher for the examined configurations with a non-stiff foundation and flexible tower. It is recommended that future work should investigate the effect of including nonlinear wave motion for better modeling of steep waves, as well as the effect of nonlinear structural response of the wind turbine.

Sammendrag

Ringing kan bli forårsaket av ikke-lineære hydrodynamiske krefter i steile bølger, av bølge-slamming, eller av brytende bølger. Denne oppgaven tar for seg den første kategorien: ikke-lineære bølgelaster på bunnfaste offshore vindturbiner i storm. To høyere ordens lastmodeller er undersøkt. FNV-modellen (Faltinsen, Newman, Vinje) tar høyde for bølgelaster på en sylinder, og inkluderer krefter til og med tredje orden av det innkommende bølgefeltet. Modellen er utledet ved en perturbasjon av den ikke-dimensjonale bølgesteilheten $kA \ll 1$, og krever at sylinderradien må være av samme orden som bølgeamplituden: $\mathcal{O}(ka) = \mathcal{O}(kA)$. De høyere ordens FNV-kreftene har sine maksimum på den frie overflaten, og minsker eksponentielt med havdybden. Raineys modell for slanke konstruksjoner er ikke utledet ved perturbasjon, men snarere ved bruk av energikonserveringsprinsipper. Det vil bli vist overensstemmelse mellom første og andre ordens krefter fra FNV og Rainey, for tilfellet med regulære bølger i dypt vann. De tredje ordens kreftene er ikke i overenstemmelse. Begge lastmodeller er utledet i denne oppgaven.

En populær programvare for dynamisk analyse av vindturbiner er åpen kildekode-programmet FAST (Fatigue, Aerodynamics, Structures and Turbulence) fra NREL (National Renewable Energy Laboratory). FAST kan produsere en tidsserieanalyse av en offshore vindturbin utsatt for diverse miljølaster. Programmet har dog kun støtte for lineære hydrodynamiske laster, så lastmodellene av interesse må bli implementert i koden. En forklaring av det teoretiske fundamentet og arkitekturen til FAST er gitt, i tillegg til detaljer vedrørende implementeringen av lastmodeller. En testcase i regulære bølger er gjennomført, med den hensikt å sammenligne individuelle lastkomponenter. Overensstemmelse mellom første og andre ordens komponenter ble påvist, som tidligere påpekt.

Dynamisk analyse av en vindturbinmodell basert på NRELs referanseturbin er gjennomført for forskjellige lastkondisjoner, operasjonstilstander og turbinkonfigurasjoner. Den første egenfrekvensen til tårnet blir holdt konstant for alle konfigurasjonene, for å unngå at den sammenfaller med rotasjonsfrekvensen til rotoren. Utslaget på toppen av turbinen ble vist å være relativt uavhengig av forskjellige tårnkonfigurasjoner og lastmodeller nær tårnets egenfrekvens. Ingen instanser av signifikant strukturrespons på grunn av høyere ordens lasteffekter ble observert. Effekten var dog høyere for de undersøkte konfigurasjonene med et ikke-stivt fundament samt et fleksibelt tårn. Det er anbefalt at fremtidig arbeid burde undersøke effekten av å inkludere ikke-lineære bølgebevegelser for å bedre kunne modellere steile bølger. Effekten av ikke-lineær strukturrespons av vindturbinen må også undersøkes.

Acknowledgments

This Master Thesis has been written during the 2014 spring semester at the Norwegian University of Science and Technology. The thesis has been submitted to partially fulfill the requirement for completing the degree of Master of Science, and has been performed at the Department of Marine Technology in Trondheim, Norway.

I would like to thank my supervisor Jørgen Ranum Krokstad, Professor at NTNU and Principal Research Engineer at Statkraft, for his guidance and dedication throughout the work with the master thesis. He arranged weekly meetings at the institute, and welcomed me at his Statkraft office when guidance was needed.

In addition, I would like to thank Lene Eliassen, Researcher at NTNU, for help with the software used in the thesis, as well as Jason Jonkman, Senior Engineer at The National Renewable Energy Laboratory, for his prompt replies to inquiries over email. A thank you also goes out to my fellow students, who have helped me overcome obstacles from day to day, and kept my motivation going. In particular, Baron Rasmus Pontus Siegmund von Ragnit was very helpful with the parts of the thesis dealing with oceanography and wave modeling.

Trondheim, June 2014

Contents

List of Figures

List of Tables

Chapter 1

Introduction

1.1 Motivation

Offshore wind turbine parks are developed at Dogger Bank outside of England. Good wind and wave conditions makes this a well suited site for offshore wind industry, but it also introduces difficult wave kinematics due to shallow water and rough loading conditions. Driving down the cost without compromising on safety is one of the main concerns for the industry, and unnecessary conservatism has to be avoided. Calculations of extreme loads are not well established in the industry, especially for dynamic structures in shallow water.

Transient structural deflections such as ringing can potentially effect a broad range of structural forms. A bottom-fixed offshore wind turbine in shallow water is a dynamic structure with a large top mass. Compared to other offshore structures, the hydrodynamic forces act relatively low on the structure, causing a short overturning moment arm. Because of these distinctive properties of the wind turbine, its vulnerability to higher order forcing effects that can cause large structural deflections has to be addressed individually.

At present, no model exists that can predict ringing accurately, and the work of developing better models and approaches to the problem is ongoing. The main motivation for writing this thesis has been to delve into the theory of some of the existing forcing models, and to examine how they relate to the study of offshore wind turbines.

1.2 Scope

The thesis is divided into three main parts. The theoretical foundation for the nonlinear forcing used throughout the thesis is given in Chapter 2. Derivations and results of the FNV (Faltinsen, Newman, Vinje) and Rainey model is given, together with a brief review of nonlinear wave motion and nonlinear structural response.

Chapter 3 reviews the architecture of the FAST (Fatigue, Aerodynamics, Structures and Turbulence) software used for dynamic analysis of wind turbines. The force models derived in Chapter 2 are implemented in FAST, and explanations of this implementation are given. The force models are compared to linear forcing for a simplified case of incident regular waves.

More realistic sea states and wind turbine configurations are applied in Chapter 4, to perform a dynamic analysis of a reference model developed by NREL (National Renewable Energy Laboratory), using the FAST software described in Chapter 3.

The scope of the thesis is to examine the effect of nonlinear forcing on bottom-fixed offshore wind turbines in storm condition. Design optimization and investigation of nonlinear effects other than nonlinear forcing will not be given.

Chapter 2

Force Models

This chapter concerns the establishing of nonlinear forcing models to predict and describe structural behavior which can not be understood on the basis of linear theory. Specifically, the forces that can cause structural ringing of offshore wind turbines will be addressed. Ringing involves excitation of the structure close to its natural frequency, and there is evidence that it occurs due to nonlinear force components of the third order of the incident waves (Tromans et al., 2006).

There has been incidents in the past of structures being exposed to higher-order forces resulting in fatal structural response, as has been confirmed by model tests of the Draugen and Heidrun offshore platforms, both revealing pronounced ringing behavior (Grue and Huseby, 2002). Methods for examining such higher-order effects needs to be established also for offshore wind turbines. Bottom-fixed offshore wind turbines situated in shallow water are however exposed to wave loads which attack lower down on the structure compared to the typical offshore platform. Thus, the overturning moment arm becomes smaller and it is therefore not clear whether higher-order effects will be as significant for the offshore wind turbines as for certain offshore structures.

Sec. 2.1 deals with linear forcing as it is described by Morison's Equation. Sec. 2.2 then deals with nonlinear forcing, and discusses higher order force components, kinematic stretching and the rationale for the choice of the two nonlinear forcing models used throughout this thesis. The first one, the FNV load model, is derived and discussed in Sec. 2.3, and the second one, the Rainey load model, is presented in Sec. 2.4. A brief introduction is given on nonlinear wave motion and nonlinear structural response, in Sec. 2.5 and Sec. 2.6 respectively, even though those components of the wave-structure interaction are not examined further in this thesis.

2.1 Linear Forcing

The conventional approach to calculating wave loads on offshore structures is by means of Morison's Equation (Morison et al., 1950). In the case of a vertical cylinder in uniaxial flow, the horizontal force is given by the following expression, consisting of an inertia term and a drag term:

$$\begin{aligned} dF^{\text{Morison}} &= dF_I^{\text{Morison}} + dF_D^{\text{Morison}} \\ &= \rho C_m \pi a^2 \frac{\partial u}{\partial t} + \rho C_d a u \left|u\right| \end{aligned} \tag{2.1}$$

where a is the cylinder radius, u is the horizontal fluid velocity, C_m is the non-dimensional added mass coefficient and C_d is the non-dimensional drag coefficient. To get the total force acting on the cylinder, Eq. 2.1 is integrated along the vertical axis, up to the mean water level. The magnitudes are illustrated in Fig. 2.1.

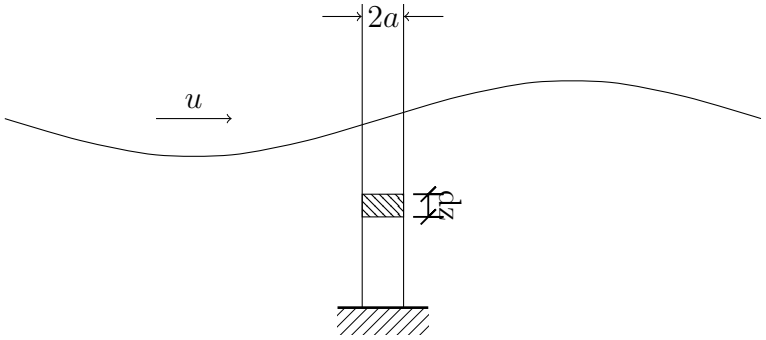

Figure 2.1: *Illustration of the parameters used in Morison's Equation.*

The inertia force resulting from Morison's Equation is calculated using the fluid velocities and accelerations at the cylinder center-line if the flow were not disturbed by the presence of the cylinder. This feature assumes inviscid flow. There is however experimental evidence of the presence of a drag force, which Morison's Equation accounts for. The sum of the theoretical inertia force and the empirical drag therefore constitutes the total force in Eq. 2.1, and it is only possible because the mechanisms that generates viscous and inviscid effects are largely independent of each other (Manners and Rainey, 1992).

Because of this distinction, the theoretical inviscid forces can be handled separately. The rest of this chapter will be devoted to ways of improving the inertia force relative to the one found in Morison's Equation.

2.2 Nonlinear Forcing

2.2.1 Higher-order Force Components

When a structure is exposed to a nonlinear wave process, it will be excited not only by the wave frequency loading, but also by the varying higher-order forces (Haver, 2009). These higher-order forces are typically much smaller in magnitude than the wave frequency forces, but they can be of importance if their excitation frequencies coincide with one of the natural frequencies of the structure.

In determining the order of magnitude of the forces, it is common to use the wave steepness as the perturbation parameter, and the non-dimensional wave slope $kA = 2\pi\frac{A}{\lambda}$ can be used as a measure for the wave steepness. Fig. 2.2 illustrates these parameters in relation to the wave steepness. The inertia term in Eq. 2.1 is of order $\mathcal{O}(kA)$ when the acceleration is written out. The purpose of Sec. 2.3 and Sec. 2.4 is to find force components of higher order, either by perturbation of the velocity potential or by energy derivations.

Specifically, the low-frequency forcing can be of importance for moored floating structures, where the natural frequency typically is smaller than the wave frequency (Greco, 2012). High-frequency forcing however, becomes important for structures with

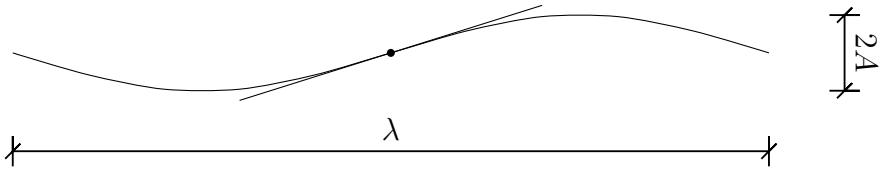

Figure 2.2: *Illustration of the wave steepness, which is the decisive for the wave force order of magnitude.*

natural frequencies higher than the wave frequency. The contribution from second-order forces can cause *springing*, which may be of importance regarding fatigue calculations (Haver, 2009), eg. fatigue accumulation in TLP tethers.

Another resonant response behavior of the structure is *ringing*, and unlike springing it may be of importance for the estimation of extreme loads. Force components of third-order are decisive for the occurrence of ringing, and ringing events typically occurs so rarely that fatigue is of less concern. In practice, it can be difficult to discern between a large springing event and a small ringing event, and other impact-type loadings such as slamming can induce resonant responses in the structure that resemble ringing (Haver, 2009).

2.2.2 Stretching

There are several ways to extrapolate the incident wave kinematics to the instantaneous free surface, in other words to predict fluid velocity and acceleration at points above the mean water level. These methods are referred to as kinematic stretching. Common methods are vertical stretching, extrapolation stretching and Wheeler stretching.

Wheeler stretching (Wheeler, 1970) is based on the observation that the velocity at the mean water level is overestimated within linear wave theory, according to DNV (2010). The vertical coordinate is stretched from the mean water level to the free surface. The relation between the original and stretched coordinate is given by

$$z = \frac{z_s - \zeta}{1 + \frac{\zeta}{d}} \tag{2.2}$$

where ζ is the wave elevation, d the water depth and z and z_s the original and stretched vertical coordinate, respectively. It can be seen from Eq. 2.2 that the wave kinematics at the free surface when using Wheeler stretching equals that of $z = 0$ with linear theory. A visualization is provided with Fig. 2.3.

Empirical observations facilitated the development and application of Wheeler stretching, and while it is mathematically inconsistent, Wheeler stretching gives good results in the region around the wave crest, but underpredicts around the mean water level $z = 0$ as well as deeper down (DNV, 2010).

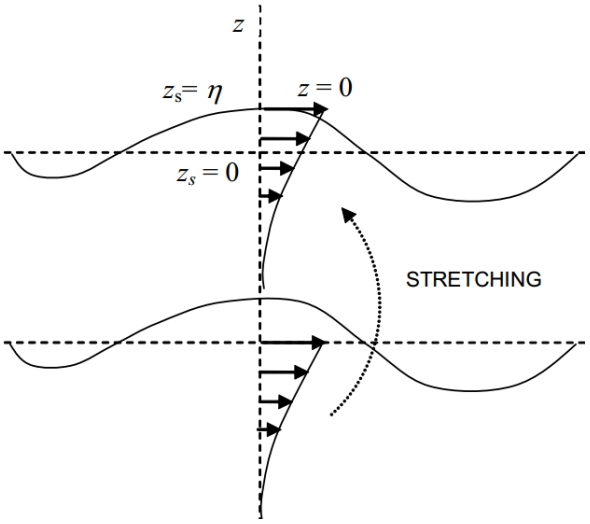

Figure 2.3: *Velocity profile using Wheeler stretching (DNV, 2010)*

2.2.3 Choice of Force Models

There are primarily two requirements when choosing a force model to describe higher order effects on a monopile offshore wind turbines in shallow water. First, the model has to be valid for extreme load cases, eg. large wave amplitudes, and second, it has to be applicable to the particular geometry of a monopile. The FNV Model (Faltinsen et al., 1995) considers the case of a vertical surface-piercing column subject to regular waves, and the Model was later extended by Newman (1996) to account for irregular waves. The model assumes a wave amplitude with the same order of magnitude as the column radius, unlike similar work by eg. Malenica and Molin (1995) which assumes that the wave amplitude is asymptotically small in relation to other length scales (Tromans et al., 2006). In a related inquiry, Rainey (1989) looked at the potential flow forces acting on a column, for the limiting case of a small radius. It will be seen that even though widely different approaches was used to derive the higher-order force components, the results obtained by FNV and Rainey are relatable.

It is recommended that model testing is used to verify numerical predictions where nonlinear forcing models are included (Haver, 2009). Due to the lack of availability of such model tests for the wind turbine analyzed in following chapters, such model testing verification is saved for future work. The next two chapters deal with the derivation of the two nonlinear force models, which are later implemented in computer code and used to investigate some of the resonant response events discussed earlier in this section.

2.3 The FNV Force Model

The motivation behind the development of the FNV model (Faltinsen et al., 1995) was the recognition that large offshore structures can experience transient response behavior at frequencies much higher than the wave excitation frequency. To describe this phenomenon, an extension to the theory of wave diffraction had to be developed. The FNV model uses a perturbation approach assuming long wave theory. Different

from the Stokes expansion, where the perturbation is performed using the small wave steepness parameter $kA = \mathcal{O}(\epsilon)$, the FNV model also assumes a column radius with the same order of magnitude as the wave amplitude: $\mathcal{O}(ka) = \mathcal{O}(kA)$. The FNV model is advocated by DNV (2010) for predicting load components up to third order of magnitude for offshore structures. The theory is derived and presented below.

2.3.1 Derivation

The Boundary Value Problem

Sea water can be assumed to be incompressible and inviscid, with the fluid motion being irrotational. The boundary value conditions for a free-surface fluid flow problem is given below (Faltinsen, 1990), starting with the field equation (Laplace equation) valid in the whole fluid domain:

$$\nabla^2\phi = 0 \quad -\infty < z < \zeta \tag{2.3}$$

For a fixed body in a moving fluid, the kinematic body boundary condition states that there will be no flow through the boundary:

$$\frac{\partial\phi}{\partial n} = 0 \quad \text{on the body surface} \tag{2.4}$$

The kinematic boundary condition on the free surface says that a fluid particle on the free-surface is assumed to stay on the free surface:

$$\frac{\partial\zeta}{\partial t} + \frac{\partial\phi}{\partial x}\frac{\partial\zeta}{\partial x} - \frac{\partial\phi}{\partial z} = 0 \quad z = \zeta \tag{2.5}$$

The dynamic free surface condition says that the water pressure equals the atmospheric pressure on the free surface, and it is derived from the Bernoulli equation:

$$g\zeta + \frac{\partial\phi}{\partial t} + \frac{1}{2}|\nabla^2\phi| = 0 \quad z = \zeta \tag{2.6}$$

If a cylinder is present, it will radiate waves, and the wave potential at infinity must be of the general form at the far field (Newman, 1977)

$$\phi \propto \frac{1}{\sqrt{r}}e^{-ikr} \quad \text{at farfield} : r \to \infty \tag{2.7}$$

where r is the distance from the origin of the cylinder, $r = \sqrt{x^2 + y^2}$.

With the kinematic free surface condition Eq. 2.5 and the dynamic free surface condition Eq. 2.6, one can not know where the free surface is before the equations are solved. By linearizing the conditions, the velocity potential becomes proportional to the wave amplitude, and is generally valid for small wave amplitudes relative to the wavelength and body dimensions. The dynamic condition resulting from linear theory (Airy wave theory) is obtained by the combination of Eq. 2.5 and Eq. 2.6, only including the linear terms.

$$\frac{\partial^2\phi}{\partial t^2} + g\frac{\partial\phi}{\partial z} = 0 \quad z = \zeta \tag{2.8}$$

The nonlinear terms can also be maintained, using nonlinear wave theory (Stokes' wave theory). Taking the material derivative of both sides of the dynamic boundary

condition Eq. 2.6 and using the kinematic boundary condition Eq. 2.5, the following combined expression can be obtained.

$$\frac{\partial^2\phi}{\partial t^2} + g\frac{\partial\phi}{\partial z} + 2\nabla\phi\nabla\frac{\partial\phi}{\partial t} + \frac{1}{2}\nabla\phi\nabla|\nabla\phi|^2 = 0 \quad z = \zeta \tag{2.9}$$

Since the free surface ζ is still unknown, a Taylor series expansion around $z = 0$ must be performed to make the boundary value problem solvable. Recall the Taylor series expansion of a function f, evaluated at $z = \zeta$, taken around the value $\zeta = 0$

$$f(x,\zeta,t) = f|_{z=0} + \zeta \left.\frac{\partial f}{\partial z}\right|_{z=0} + \frac{1}{2}\zeta^2\left.\frac{\partial^2 f}{\partial z^2}\right|_{z=0} + \dots \tag{2.10}$$

Performing the expansion in Eq. 2.10 on the nonlinear dynamic condition Eq. 2.9 gives

$$\frac{\partial^2\phi}{\partial t^2} + g\frac{\partial\phi}{\partial z} + \zeta\frac{\partial}{\partial z}\left(\frac{\partial^2\phi}{\partial t^2} + g\frac{\partial\phi}{\partial z}\right) + 2\nabla\phi\nabla\frac{\partial\phi}{\partial t} = 0 \quad z = 0 \tag{2.11}$$

showing terms up to double products of ζ and ϕ, representing the Stokes expansion up to second order $\mathcal{O}((kA)^2)$, where kA is the wave steepness, which is of small magnitude in long wave theory: $kA = \mathcal{O}(\epsilon)$.

In general, the exact solution of the boundary value problem is approximated using a so called perturbation series approach. The series expansion are in terms of the small perturbation parameter ϵ proportional to the wave steepness. Thus, the potential and surface elevation can be written on the form

$$\phi = \epsilon\phi_1 + \epsilon^2\phi_2 + \epsilon^3\phi_3 + \dots \tag{2.12}$$

$$\zeta = \epsilon\zeta_1 + \epsilon^2\zeta_2 + \epsilon^3\zeta_3 + \dots \tag{2.13}$$

The Stokes second order dynamic equation derived in Eq. 2.11 can likewise be represented by a perturbation on the form

$$\begin{aligned}\epsilon\left\{\frac{\partial^2\phi}{\partial t^2} + g\frac{\partial\phi}{\partial z}\right\} + \epsilon^2\left\{\frac{\partial^2\phi}{\partial t^2} + g\frac{\partial\phi}{\partial z} + \right.\\ \left.\zeta\frac{\partial}{\partial z}\left(\frac{\partial^2\phi}{\partial t^2} + g\frac{\partial\phi}{\partial z}\right) + 2\nabla\phi\nabla\frac{\partial\phi}{\partial t}\right\} + \mathcal{O}(\epsilon^3) = 0 \quad z = 0\end{aligned} \tag{2.14}$$

where each term on the left hand side needs to be zero separately.

The next sections are used to establish the potential up to the third order. The derivations requires a significant amount of complicated mathematics, and are only carried out in detail when it is appropriate to do so with respect to the scope of this thesis. Otherwise the results are merely presented.

Linear Potential

Sea Loads on Ships and Offshore Structures (Faltinsen, 1990) gives the velocity potential for a wave in infinite water depth ($h > \frac{1}{2}\lambda$), where the dispersion relation holds, $k = \omega^2/g$. This is not true at offshore wind parks like Dogger Bank, where h is no larger than approximately $50m$, but it is nevertheless assumed in the following derivation. The insights derived from deep water analysis may prove useful when later

extending the theory to shallow water conditions. The velocity potential is given in Eq. 2.15 below.

$$\phi = \frac{gA}{\omega} e^{kz} \cos(\omega t - kx) \tag{2.15}$$

The diffraction potential ϕ_D can be divided into a component ϕ_I describing the incoming wave field, and a component ϕ_S describing the scattered waves around the cylinder. Looking at the incoming potential, and using complex notation, Eq. 2.15 can be written as

$$\phi_I = \Re \left\{ \frac{gA}{\omega} e^{kz - ikx + i\omega t} \right\} \tag{2.16}$$

Equation Eq. 2.16 can be better dealt with by writing it in cylindrical coordinates (r, θ). $r = 0$ at the cylinder axis and $\theta = 0$ in the direction of wave propagation. The conversion between Cartesian and cylindrical coordinates is given by $x + iy = re^{i\theta}$, where $x = r\cos\theta$ and $y = r\sin\theta$.

The theory of Bessel functions is given in Advanced Engineering Mathematics (Kreyszig, 2006). Bessel's equation is an ODE that appears in a diverse range of applications, but especially when cylindrical symmetry can be identified. The Bessel function of the first kind of order n is given as

$$J_n(x) = x^n \sum_{m=0}^{\infty} \frac{(-1)^m x^{2m}}{2^{2m+n} m!(n+m)!} \tag{2.17}$$

It is desirable to write the potential in terms of Bessel functions. Doing a Taylor expansion on the e^{-ikx} term in Eq. 2.16 yields

$$\begin{aligned}
e^{-ikx} &= e^{-ikr\cos\theta} = e^{-ikr\frac{e^{i\theta}+e^{-i\theta}}{2}} = e^{\frac{\zeta}{2}(\eta - 1/\eta)} = e^{\frac{\zeta}{2}\eta} \times e^{-\frac{\zeta}{2}\frac{1}{\eta}} \\
&= \sum_{n=0}^{\infty} \frac{1}{n!} \left(\frac{\zeta\eta}{2}\right)^n \times \sum_{m=0}^{\infty} \frac{1}{m!} \left(-\frac{\zeta}{2\eta}\right)^m \\
&= \sum_{n=-\infty}^{\infty} \eta^n \left(\frac{(\zeta/2)^n}{n!} - \frac{(\zeta/2)^{n+2}}{1!(n+1)!} + \frac{(\zeta/2)^{n+4}}{2!(n+2)!} + \ldots + (-1)^k \frac{(\zeta/2)^{n+2k}}{k!(n+k)!} \right) \\
&= \sum_{n=-\infty}^{\infty} \eta^n J_n(\zeta) \\
&= \sum_{n=-\infty}^{\infty} (-i)^n J_n(kr) e^{-in\theta}
\end{aligned} \tag{2.18}$$

where $\zeta = kr$ and $\eta = -ie^{-i\theta}$ was used to simplify the derivation. Now, dividing the final sum in Eq. 2.18 into two terms, and applying the identities $J_{-n}(x) = (-1)^n J_n(x)$

and $(-i)^{-n} = (-1)^n i^{-n}$ (Kreyszig, 2006), the following relation can be derived.

$$\begin{aligned} e^{-ikx} &= \sum_{n=-\infty}^{-1} (-i)^n J_n(kr) e^{-in\theta} + \sum_{n=0}^{\infty} (-i)^n J_n(kr) e^{-in\theta} \\ &= \sum_{n=1}^{\infty} (-i)^{-n} J_{-n}(kr) e^{in\theta} + \sum_{n=0}^{\infty} (-i)^n J_n(kr) e^{-in\theta} \\ &= J_0(kr) + \sum_{n=1}^{\infty} i^{-n} J_n(kr)(e^{in\theta} + e^{-in\theta}) \\ &= J_0(kr) + 2\sum_{n=1}^{\infty} i^{-n} J_n(kr) \cos n\theta \\ &= \sum_{n=0}^{\infty} \epsilon_n i^{-n} J_n(kr) \cos n\theta \end{aligned} \tag{2.19}$$

where ϵ_n is defined as

$$\epsilon_n = \begin{cases} 1 & \text{if } n = 0 \\ 2 & \text{if } n > 0 \end{cases} \tag{2.20}$$

Combining Eq. 2.16 and Eq. 2.19 gives

$$\phi_I = \Re \left\{ \frac{gA}{\omega} e^{kz + i\omega t} \sum_{n=0}^{\infty} \epsilon_n i^{-n} J_n(kr) \cos n\theta \right\} \tag{2.21}$$

which is the formula for the incoming velocity potential found in Faltinsen et al. (1995).

Now consider the diffraction of waves by a fixed vertical cylinder, representing the wind turbine tower. In the following, consider linear wave theory assuming small surface elevation relative to the wave length, as well as a small cylinder radius relative to the wave length. Furthermore, the wave amplitude A and the cylinder radius a are of the same order, (Faltinsen et al., 1995). This has been known as FNV theory, and is valid for a fixed vertical cylinder of uniform diameter, which is penetrating the water surface and is situated in infinite water depth.

$$\begin{aligned} kA &= \mathcal{O}(\epsilon) \ll 1 \\ ka &= \mathcal{O}(kA) = \mathcal{O}(\epsilon) \ll 1 \end{aligned} \tag{2.22}$$

Due to the presence of the cylinder, the scattered linear potential ϕ_S has to be found. Rewriting the Laplace equation Eq. 2.3 in terms of cylindric coordinates yields:

$$\nabla^2 \phi_S = \frac{\partial^2 \phi_S}{\partial r^2} + \frac{1}{r}\frac{\partial \phi_S}{\partial r} + \frac{1}{r^2}\frac{\partial^2 \phi_S}{\partial \theta^2} + \frac{\partial^2 \phi_S}{\partial z^2} = 0 \tag{2.23}$$

Also using the kinematic body boundary condition on the cylinder wall Eq. 2.4

$$\frac{\partial \phi_D}{\partial r} = \frac{\partial \phi_I}{\partial r} + \frac{\partial \phi_S}{\partial r} = 0 \implies \frac{\partial \phi_I}{\partial r} = -\frac{\partial \phi_S}{\partial r}, \quad r = a \tag{2.24}$$

and together with the radiation condition in Eq. 2.7, the scattered velocity potential can be found.

Without knowing the exact expression for the scattered potential yet, the general form can be described by Eq. 2.25 below

$$\phi_S = \Re\left\{\frac{gA}{\omega}e^{kz+i\omega t}\gamma(r,\theta)\right\} \tag{2.25}$$

where $\gamma = P(r)Q(\theta)$ is a separable function in r and θ (Olsen, 2010). By substituting Eq. 2.25 into the Laplace equation Eq. 2.23, and solving the differential equation by separation, one gets

$$P_n(kr) = B_n J_n(kr) + C_n Y_n(kr) \tag{2.26}$$
$$Q(\theta) = A_1 \cos n\theta + A_2 \sin n\theta \tag{2.27}$$

where A_n, B_n and C_n are constants, n a positive integer and Y_n the Bessel function of second kind. The simple equations in Eq. 2.26 and Eq. 2.27 proves the advantage of using Bessel theory on problems with cylindrical symmetry. A_2 is set to zero because the sine term is antisymmetric around the x-axis, which disagrees with the physics of the problem of a uniaxial flow in x-direction. To satisfy the radiation condition Eq. 2.7, B and C should be chosen so that the function

$$P_n(kr) = B_n^* J_n(kr) - iC_n^* Y_n(kr) \tag{2.28}$$

is satisfying the far field radiation condition Eq. 2.7

$$P_n(kr) \propto \frac{1}{\sqrt{kr}}(\cos kr - i\sin kr) = \frac{1}{\sqrt{kr}}e^{-ikr} \quad kr \to \infty \tag{2.29}$$

according to the asymptotic expansion of the Bessel functions.

The so called Hankel functions (Kreyszig, 2006) are useful in the following derivations, and the Hankel function of the second kind is defined as

$$H_n^{(2)} = J_n - iY_n \tag{2.30}$$

and Eq. 2.28 can now be written as

$$P_n(kr) = D_n H_n^{(2)}(kr) \tag{2.31}$$

where D_n is a complex constant able to represent Eq. 2.28. By setting the derived components of $\gamma = P(r)Q(\theta)$ into Eq. 2.25, the scattered potential now becomes:

$$\phi_S = \Re\left\{\frac{gA}{\omega}e^{kz+i\omega t}\sum_{n=0}^{\infty} D_n \cos n\theta H_n^{(2)}(kr)\right\} \tag{2.32}$$

The constant D_n is found by applying the kinematic boundary condition Eq. 2.24, which gives

$$D_n = -\epsilon_n i^{-n}\frac{1}{\partial H_n^{(2)}(ka)/\partial(ka)}\frac{\partial J_n(ka)}{\partial(ka)} \tag{2.33}$$

Hence, the linear scattered velocity potential is derived

$$\phi_S = -\Re\left\{\frac{gA}{\omega}e^{kz+i\omega t}\sum_{n=0}^{\infty}\epsilon_n i^{-n}\cos n\theta H_n^{(2)}(kr)\frac{\partial J_n/\partial(ka)}{\partial H_n^{(2)}/\partial(ka)}\right\} \tag{2.34}$$

The total linear potential is then the sum of the incident wave potential and the scattered potential

$$\begin{aligned}\phi_D &= \phi_I + \phi_S \\ &= \Re\left\{\frac{gA}{\omega}e^{kz+i\omega t}\sum_{n=0}^{\infty}\epsilon_n i^{-n}\cos n\theta\left(J_n(kr) - H_n^{(2)}(kr)\frac{J_n'(ka)}{H_n^{(2)\prime}(ka)}\right)\right\}\end{aligned} \tag{2.35}$$

as given in Faltinsen et al. (1995).

The domain is divided into two regions: the inner and outer domain. $kr = \mathcal{O}(\epsilon) \ll 1$ in the inner domain, and $kr = \mathcal{O}(1)$ in the outer domain. The sub domains are treated one at a time. Now that Eq. 2.35 is established, it is time to evaluate the Bessel functions corresponding to the leading terms of the potential. Starting with the scattered potential, and rewriting Eq. 2.34 into a more convenient form.

$$\phi_S = -\Re\left\{\frac{gA}{\omega}e^{kz+i\omega t}\hat{\phi}_S\right\} \tag{2.36}$$

In the outer domain, using the expansions of the Bessel and Hankel functions of argument ka when $ka = \mathcal{O}(\epsilon)$, the dominant terms are the ones when $m = 0, 1$ (Faltinsen et al., 1995)

$$\hat{\phi}_S = -\frac{i\pi(ka)^2}{4}\left(H_0^{(2)}(kr) + i2\cos\theta H_1^{(2)}(kr)\right) \tag{2.37}$$

Likewise, for the inner domain, using the expansions of the Bessel and Hankel functions of argument kr when $kr = \mathcal{O}(\epsilon)$, the dominant term is from $m = 1$

$$\hat{\phi}_S = i\frac{ka^2}{r}\cos\theta \tag{2.38}$$

The leading terms of the expansion of Bessel functions for the incoming potential $\hat{\phi}_I$ in the inner domain is also evaluated

$$\hat{\phi}_I = 1 - ikr\cos\theta \tag{2.39}$$

Combining Eq. 2.38 and Eq. 2.39 results in the total potential for the inner domain up to an order of ϵ^2 yields

$$\phi_D = \Re\left\{\frac{gA}{\omega}e^{kz+i\omega t}\left[1 - ik\cos\theta\left(r + \frac{a^2}{r}\right)\right]\right\} + \mathcal{O}(\epsilon^3) \tag{2.40}$$

Doing the same analysis but including terms up to the order of ϵ^3, the total potential is finally given as:

$$\begin{aligned}\phi_D = \Re\Bigg\{\frac{gA}{\omega}e^{kz+i\omega t}\Bigg[1 &- ik\cos\theta\left(r + \frac{a^2}{r}\right) - \frac{1}{4}(kr)^2 \\ &+ \frac{1}{2}(ka)^2\left(\log\frac{1}{2}kr + C + \frac{i\pi}{2}\right) \\ &- \frac{1}{4}k^2\cos 2\theta\left(r^2 + \frac{a^4}{r^2}\right)\Bigg]\Bigg\} + \mathcal{O}(\epsilon^4)\end{aligned} \tag{2.41}$$

Nonlinear Potential

Recall that the wave amplitude A is of the same order of magnitude as the cylinder radius a. Equation Eq. 2.41 includes terms of order $Aa^2 = \mathcal{O}(\epsilon^3)$, but nonlinear terms of order A^2a and A^3 are ignored in the linear solution. To compensate for this inconsistency, a correction is included in the total potential for the inner domain

$$\phi = \phi_D + \psi + \mathcal{O}(\epsilon^4) \tag{2.42}$$

The boundary conditions for ψ is the same as for ϕ,

$$\frac{\partial \psi}{\partial r} = 0 \quad \text{at } r = a \tag{2.43}$$

$$\frac{\partial^2 \psi}{\partial t^2} + g\frac{\partial \psi}{\partial z} = -2\nabla\phi\nabla\phi_t - \frac{1}{2}\nabla\phi\nabla(\nabla\phi)^2 \quad \text{at } z = \zeta \tag{2.44}$$

which is the kinematic body boundary condition and the dynamic free surface condition, respectively.

$\nabla\phi_i\nabla\phi_j$ can be found for i and $j \in (I, S)$ which in turn solves the two terms on the right side of Eq. 2.44, both deriving from Eq. 2.40 with order of magnitude $\mathcal{O}(\epsilon^2)$.

$$-2\nabla\phi\nabla\phi_t = \omega^3 A^2 e^{2kz} \sin 2\omega t \left(\frac{2a^2}{r^2}\cos 2\theta - \frac{a^4}{r^4}\right) + \mathcal{O}(\epsilon^3) \tag{2.45}$$

$$\begin{aligned} &-\frac{1}{2}\nabla\phi\nabla(\nabla\phi)^2 = \\ &-2\omega^3 A^3 e^{3kz}\sin^3\omega t\left(\frac{a^2}{r^3}\cos 3\theta - 2\frac{a^4}{r^5}\cos\theta + \frac{a^6}{r^7}\cos\theta\right) + \mathcal{O}(\epsilon^3) \end{aligned} \tag{2.46}$$

Before Eq. 2.43 and Eq. 2.44 are used to find ψ, it is better to normalize r and z in terms of the inner coordinates.

$$R \stackrel{\text{def}}{=} \frac{r}{a} \tag{2.47}$$

$$Z \stackrel{\text{def}}{=} \frac{-z + A\sin\omega t}{a} \tag{2.48}$$

$Z = 0$ oscillates with the first order wave elevation ζ. The nonlinear inner potential in inner coordinates must fulfill

$$\Psi(R, \theta, Z) \stackrel{\text{def}}{=} \psi(r, \theta, z) \tag{2.49}$$

The boundary conditions Eq. 2.43 and Eq. 2.44 are still valid for the potential in inner coordinates, but the differential operators needs to be changed according to Eq. 2.47 and Eq. 2.48. The combined result is given in Faltinsen et al. (1995).

$$\begin{aligned} &\frac{a}{g}\Psi_{tt} + 2\omega\frac{A}{g}\cos\omega t\Psi_{Zt} - kA\sin\omega t\Psi_Z + kA\frac{A}{a}\cos^2\omega t\Psi_{ZZ} - \Psi_Z = \\ &\omega kaA^2\sin 2\omega t\left(\frac{2}{R^2}\cos 2\theta - \frac{1}{R^4}\right) - \\ &\omega kA^3\sin^3\omega t\left[\frac{2}{R^3}\cos 3\theta + \left(-\frac{4}{R^5} + \frac{2}{R^7}\right)\cos\theta\right] \end{aligned} \tag{2.50}$$

The three first terms on the left hand side of Eq. 2.50 is of order $\mathcal{O}(\epsilon^4)$ and can therefore be omitted from the solution, since a third order nonlinear potential derivative is wanted.

$$\begin{aligned}\Psi_Z = &-\omega k a A^2 \sin 2\omega t \left(\frac{2}{R^2}\cos 2\theta - \frac{1}{R^4}\right) + \\ &\omega k A^3 \sin^3 \omega t \left[\frac{2}{R^3}\cos 3\theta + \left(-\frac{4}{R^5} + \frac{2}{R^7}\right)\cos\theta\right]\end{aligned} \tag{2.51}$$

Given Eq. 2.51, the solution of Ψ can be assumed to take on the following form (Faltinsen et al., 1995)

$$\Psi(r, z, t) = \sum_{m=0}^{3} c_m(t)\Psi_m(R, Z)\cos m\theta \tag{2.52}$$

where the c's are time dependent factors taken from Eq. 2.51,

$$c_0 = c_2 = \omega k A^2 a \sin 2\omega t \tag{2.53}$$

$$c_1 = c_3 = \omega k A^3 \sin^3 \omega t \tag{2.54}$$

and the Ψ_m's are non-dimensional functions, subjected to the boundary condition of

$$\Psi_{mZ}(R, 0) = f_m(R) \quad \text{outside of the cylinder} \tag{2.55}$$

$$f_0 = \frac{1}{R^4}, \quad f_1 = -\frac{4}{R^5} + \frac{2}{R^7}, \quad f_2 = -\frac{2}{R^2}, \quad f_3 = \frac{2}{R^3} \tag{2.56}$$

The evaluation of the f-s, the forcing functions, are done by separation of variables with Weber transforms of Eq. 2.51, and is saved for future study. Numerical values for the functions Ψ_m is given by Newman and Lee (1995) in a paper discussing runup on a vertical cylinder, and therefore the results are only given for $Z = 0$, ie. on the first order linear free surface, and $R = 1$, ie. on the cylinder wall. The results are reproduced in Table 2.1.

m	$\Psi_m(R = 1, Z = 0)$
0	-0.5755
1	0.8004
2	0.8091
3	-0.4925

Table 2.1: Ψ_m *on the cylinder wall and on the linear free surface*

Forces due to Regular Waves

The total integrated force acting on the cylinder due to dynamic pressure from the water is (Faltinsen et al., 1995)

$$\begin{aligned}F_x &= -a\int_0^{2\pi}\cos\theta d\theta \int_{-\infty}^{\zeta} p(a, \theta, z, t)dz \\ &= \rho a \int_0^{2\pi}\cos\theta d\theta \int_{-\infty}^{\zeta}\left(\phi_t + \frac{1}{2}V^2 + gz\right)\Big|_{r=a} dz\end{aligned} \tag{2.57}$$

The force distribution per length unit dz is called the differential force and is given by

$$F' = -a \int_0^{2\pi} p \cos\theta d\theta \tag{2.58}$$

which is the force differentiated with respect to the vertical direction z. This differential force is useful as a tool for finding the wave loads on a cylinder in finite water depth, where it can be assumed that the pressure field near the free surface equals that of a cylinder in infinite fluid.

When evaluating Eq. 2.57, it is useful to divide the region of integration into two sub domains. The reason for this is the variation of $z = \zeta$, so that one of the sub domains should handle what happens below the still water line and vice versa.

$$\begin{aligned} F_x =& \rho a \int_0^{2\pi} \cos\theta d\theta \int_{-\infty}^{0} \left(\phi_t + \frac{1}{2}V^2\right)\Big|_{r=a} dz + \\ & \rho a \int_0^{2\pi} \cos\theta d\theta \int_0^{\zeta} \left(\phi_t + \frac{1}{2}V^2 + gz\right)\Big|_{r=a} dz \end{aligned} \tag{2.59}$$

In the first integral the term gz is not included since it does not contribute to the integral over θ.

Using the first order term from the potential found in Eq. 2.41, and considering only the first order term of the pressure in Eq. 2.58, the first order differential force can easily be found.

$$F_1' = \rho a \int_0^{2\pi} \phi_{Dt} \cos\theta d\theta = 2\pi\rho g k A a^2 e^{kz} \cos\omega t \tag{2.60}$$

This is equal to the inertia part of the Morison equation Eq. 2.1 when $V = \pi a^2 dz$ and $C_m = 2$. The second order component is found in the same way, by considering the second order term in Eq. 2.58.

$$F_2' = \rho a \int_0^{2\pi} \frac{1}{2}(\nabla\phi_D)^2 \cos\theta d\theta = \frac{1}{2}\pi\rho g k^2 a^2 A^2 e^{2kz} \sin 2\omega t \tag{2.61}$$

The nonlinear potential from Eq. 2.42 gives a contribution to the pressure equal to

$$p = -\rho(\psi_t + \nabla\phi_D \nabla\psi) \tag{2.62}$$

and the corresponding differential force of third order becomes

$$\begin{aligned} F_3' &= \rho a \int_0^{2\pi} (\psi_t + \nabla\phi_D\nabla\psi)\cos\theta d\theta \\ &= \frac{\pi}{2}\rho g k^2 A^3 a(\cos\omega t - \cos 3\omega t) \times \left(\frac{3}{2}\Psi_1(1,Z) + 2\Psi_2(1,Z)\right) \end{aligned} \tag{2.63}$$

The linear potentials were given in Table 2.1 for $Z = 0$.

Next, consider the contribution from the second term in the integrated force in Eq. 2.59. The first order wave elevation $\zeta_1 = A\sin\omega t$ is not dependent on θ and the force can thus be evaluated directly from Eq. 2.60, Eq. 2.61 and Eq. 2.63.

$$\tilde{F}_i = \int_0^{\zeta_1} F_i' dz \tag{2.64}$$

which can be thought of as point forces acting within the free surface region. That is to say when $r = \mathcal{O}(\epsilon)$.

Gathering all the contributions, the total point force acting on the cylinder is given by the expression

$$\tilde{F}_x = \pi\rho g k a^2 A^2 \sin 2\omega t + \pi\rho g k^2 a^2 A^3(\cos\omega t - 2\cos 3\omega t) + \mathcal{O}(\epsilon^6) \tag{2.65}$$

and the expression for the total integrated force on the cylinder is (Olsen, 2010)

$$\begin{aligned} F_x =& \pi\rho g \cos\omega t(2Aa^2 + k^2A^3a^2) + \frac{5}{4}\pi\rho g k A^2 a^2 \sin 2\omega t \\ & - 2\pi\rho g k^2 A^3 a^2 \cos 3\omega t + \mathcal{O}(\epsilon^6) \end{aligned} \tag{2.66}$$

Forces due to Irregular Waves

In reality the sea surface is irregular, and has to be described by a combination of regular waves with different directions, amplitudes an frequencies (Myrhaug, 2007). For long crested waves the regular waves are assumed to propagate in the same direction and can be written as a sum of all the regular components.

$$\zeta(x,t) = \sum_{n=1}^{N} A_n \cos\left(\omega_n t - k_n x + \epsilon_n\right) \tag{2.67}$$

where ϵ_n are stochastic independent rectangular distributed (between 0 and 2π) phase constants. Looking at the case of short crested waves, we have a double sum of regular components.

$$\zeta(x,y,t) = \sum_{i=1}^{I}\sum_{j=1}^{J} A_{ij} \cos\left(\omega_i t - k_i x\cos\theta_j - k_i y \sin\theta_j + \epsilon_{ij}\right) \tag{2.68}$$

The total energy of all the regular wave components is given by

$$\frac{E}{\rho g} = \sum_{i=1}^{I}\sum_{j=1}^{J} \frac{1}{2} A_{ij}^2 = \sum_{i=1}^{I}\sum_{j=1}^{J} S(\omega_i,\theta_j)\Delta\omega\Delta\theta \tag{2.69}$$

and letting $I, J \to \infty$ and $\Delta\omega, \Delta\theta \to 0$ one obtains a continuous spectrum which describes the concentration of energy per frequency interval.

$$\frac{E}{\rho g} = \int_0^{2\pi}\int_0^{\infty} S(\omega,\theta)d\omega d\theta \tag{2.70}$$

where the spectrum $S(\omega)$ can be found by integrating over the directional spectrum $S(\omega,\theta)$.

Newman (1996) made the FNV theory presented in the above sections applicable for unidirectional irregular waves. A basic assumption of this extension (like it was in the regular case) is that the wavelength of each spectral component is large compared to the cylinder radius and the wave amplitude of the component. According to Newman the most significant high-frequency loads in irregular waves comes from the scattering of waves by the cylinder, and not from nonlinear effects in the incident wave field.

The linear potential in Eq. 2.16 can be extended to irregular waves by summing over the components.

$$\phi_I = \sum_{n=1}^{N} \Re\left\{ \frac{gA_n}{\omega_n} e^{k_n z - ik_n x + i\omega_n t} \right\} \tag{2.71}$$

where A_n is the complex and describes amplitude with the length $|A_n|$ and phase shift ϵ_n with the argument $\arg(A_n)$. The wave elevation is likewise a sum of components. Looking at the kinematic boundary condition at the free surface Eq. 2.5, it includes a nonlinear product of these two sums. Hence, the following identity for two complex expressions will be useful

$$\Re\{K_1\}\Re\{K_2\} = \frac{1}{2}\left(\Re\{K_1 K_2\} + \Re\{K_1 K_2^*\}\right) \tag{2.72}$$

where K_2^* is the complex conjugate. Trigonometric identities can be used to find the products of the two expressions, and by summing over all these products, the potential can be found for irregular waves.

Using the expression for the total integrated force in Eq. 2.90, the horizontal forces acting on the cylinder can be found, using Bernoulli's Equation to evaluate the pressure.

The first and second order differential forces is then found and given in Eq. 2.73 and 2.74 below.

$$F_1' = 2\pi\rho a^2 u_t \tag{2.73}$$

$$F_2' = \pi\rho a^2(2ww_x + uu_x) \tag{2.74}$$

The differential forces are integrated up to the mean surface to get the forces acting on the cylinder.

The third order differential force from the nonlinear potential corresponding to the one found in Eq. 2.63 is given in Eq. 2.75 below for irregular waves (Newman, 1996)

$$F_3'(Z) = \frac{\pi\rho a}{g} u^2 u_t (3\Psi_1 + 4\Psi_2) \tag{2.75}$$

which integrated along the length of the vertical coordinate of a column in infinite depth becomes

$$\begin{aligned} F_3^{(\Psi)} &= \frac{\pi\rho a}{g} u^2 u_t \int_0^\infty (3\Psi_1 + 4\Psi_2) dZ \\ &= 4\frac{\pi\rho a}{g} u^2 u_t \end{aligned} \tag{2.76}$$

where the superscript Ψ denotes that it is based on the nonlinear potential.

The remaining point forces at surface intersection are found by integration of the differential forces up to the free surface, as was shown in Eq. 2.64. Integrating the first and second differential force gives Eq. 2.77 below (Newman, 1996).

$$\begin{aligned} \tilde{F}_1 + \tilde{F}_2 &= \int_0^\zeta (F_1 + F_2) dz \\ &= \pi\rho a^2 \left[\zeta \left(2u_t - \frac{2}{g} u_t w_t + u_t z\zeta + 2ww_x + uu_x \right) - \frac{u_t}{g}(u^2 + w^2) \right] \end{aligned} \tag{2.77}$$

In Eq. 2.77 there are terms of second order and terms of third order due to the linear potential. All the horizontal force components are now established, and summarized in the next section.

2.3.2 Result

Using Eq. 2.73, 2.74, 2.76 and 2.77, the formulas are here reproduced and grouped into orders of magnitude of the wave steepness of the incoming wave field, denoted by the subscripts. For the third order forces, a distinction is made between those emerging from the linear potential ϕ, and those from the nonlinear potential Ψ. All the point loads are lumped down to the mean surface, using the velocity components at $z = 0$. Even though the FNV model was developed assuming infinite water depth, the integration is here performed along the finite depth of the cylinder, to make it applicable to practical problems.

$$F_1 = 2\pi\rho a^2 \int_{-d}^{0} u_t dz \tag{2.78}$$

$$F_2 = \pi\rho a^2 \int_{-d}^{0} (2ww_x + uu_x)dz + 2\pi\rho a^2 u_t \zeta \tag{2.79}$$

$$F_3^{(\phi)} = \pi\rho a^2 \left[\zeta \left(u_{tz}\zeta + 2ww_x + uu_x - \frac{2}{g} u_t w_t \right) - \frac{u_t}{g}(u^2 + w^2) \right] \tag{2.80}$$

$$F_3^{(\Psi)} = 4\frac{\pi\rho a}{g} u^2 u_t \tag{2.81}$$

These results correspond to those given by Newman (1996).

2.4 The Rainey Force Model

Rainey (1989) derived equations for the wave loading on a moving lattice-type offshore structure. These equations can be applied to the special case of a fixed partial immersed cylinder, representing the wind turbine tower. The theory proposed by Rainey requires a small cylinder diameter (slender body theory), and the fluid properties are only dealt with at the cylinder centerline.

The expressions for calculating the wave loads are summarized by Rainey (1995) in a paper that generalizes those expressions to account for a structure of non-circular member cross-sections, joints between members, and surface intersections. Only some of these expressions apply to the single member wind turbine tower. Rainey's slender body forces are not based on a perturbation expansion like the one used to derive forces according to FNV theory, but rather derived from energy considerations.

In the following, the distributed components of the Rainey equation will be derived by taking another approach than what was done in the original paper: a perturbation approach is used. The point load at surface intersection is merely presented. At first, uniaxial wave propagation in the x-direction will be considered, and the resulting horizontal force on a slender fixed vertical cylinder will be given. The expressions will thereafter be generalized and written on matrix form, for easier implementation in computer code.

2.4.1 Derivation

A three-dimensional slender cylinder is shown in Fig. 2.4. The cylinder is placed in an undisturbed fluid flow assumed to be incompressible, inviscid and irrotational, in other

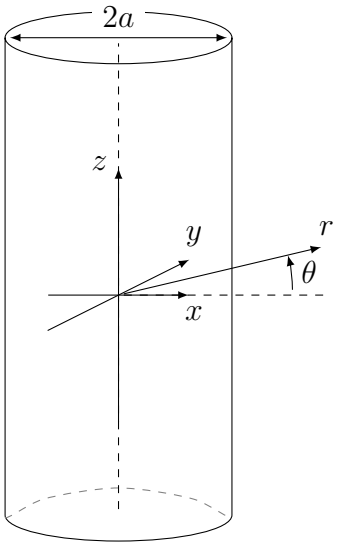

Figure 2.4: *Axis system for the slender cylinder representing the wind turbine tower, given both in cartesian coordinates and polar coordinates. The cylinder radius is a.*

words a potential flow. Thus, the velocities of the flow can be found from the spatial derivatives of the potential $\phi = \phi(x, y, z, t)$. An expression for the potential including second-order terms needs to be found, using a Taylor series expansion around the origin, the origin being the cylinder centerline at the mean water level $z = 0$. Kreyszig (2006) gives the expression for a one-dimensional Taylor expansion around zero

$$f(z) = \sum_{n=0}^{\infty} \frac{z^n}{n!} \times \left. \frac{d^n f}{dz^n} \right|_{z=0} \tag{2.82}$$

which can be generalized to functions of more than one variable:

$$f(x_1, \ldots, x_d) = \sum_{n_1=0}^{\infty} \sum_{n_2=0}^{\infty} \cdots \sum_{n_d=0}^{\infty} \frac{x_1^{n_1} x_2^{n_2} \ldots x_d^{n_d}}{n_1! n_2! \ldots n_d!} \times \left. \frac{\partial^{n_1+n_2+\cdots+n_d} f}{\partial x_1^{n_1} \partial x_2^{n_2} \ldots \partial x_d^{n_d}} \right|_{x_1,\ldots,x_d=0} \tag{2.83}$$

still expanding around the zero value of each variable.

By using Eq. 2.83 and only including terms up to second order of each of the three spatial variables, the potential ϕ can be written on the more convenient form (Manners and Rainey, 1992):

$$\begin{aligned} \phi(x, y, z, t) = \phi_0 &+ D_{100}x + D_{010}y + D_{001}z + \frac{1}{2}D_{200}x^2 + \frac{1}{2}D_{020}y^2 + \frac{1}{2}D_{002}z^2 \\ &+ D_{110}xy + D_{101}xz + D_{011}yz \end{aligned} \tag{2.84}$$

The Ds are functions evaluated at the origin and defined by the relation

$$D_{abc} = \frac{\partial^{a+b+c}\phi}{\partial x^a \partial y^b \partial z^c} \tag{2.85}$$

Eq. 2.84 can be further simplified by using the Laplace equation $\nabla^2\phi = 0 \rightarrow D_{200} + D_{020} + D_{002} = 0$ and using this to eliminate D_{020} from the equation, $D_{020} = -(D_{200} +$

D_{002}). The introduction of polar coordinates will also make Eq. 2.84 easier to handle. Eq. 2.86 gives the transformations from Cartesian coordinates to polar coordinates.

$$\begin{aligned} x &= r\cos\theta \\ y &= r\sin\theta \end{aligned} \tag{2.86}$$

The final expression for the undisturbed potential up to second order, using polar coordinates, is derived in Eq. 2.87.

$$\begin{aligned} \phi &= \phi_0 + D_{100}x + D_{010}y + D_{001}z + \frac{1}{2}D_{200}(x^2 - y^2) + \frac{1}{2}D_{002}(z^2 - y^2) \\ &\quad + D_{110}xy + D_{101}xz + D_{011}yz \\ &= \phi_0 + D_{100}r\cos\theta + D_{010}r\sin\theta + D_{001}z + \frac{1}{2}D_{200}r^2\cos 2\theta \\ &\quad + \frac{1}{2}D_{002}(z^2 - r^2\sin^2\theta) + \frac{1}{2}D_{110}r^2\sin 2\theta + D_{101}zr\cos\theta + D_{011}zr\sin\theta \\ &= \phi_0 + D_{001}z + \frac{1}{4}D_{002}(2z^2 - r^2) + (D_{100} + D_{101}z)r\cos\theta \\ &\quad + (D_{010} + D_{001}z)r\sin\theta + \frac{1}{4}(2D_{200} + D_{002})r^2\cos 2\theta + \frac{1}{2}D_{110}r^2\sin 2\theta \end{aligned} \tag{2.87}$$

The trigonometric identities used in the derivation of Eq. 2.87 are: $\sin^2\theta + \cos^2\theta = 1$, $\sin 2\theta = 2\sin\theta\cos\theta$, $\cos 2\theta = \cos^2\theta - \sin^2\theta$ and $\cos^2\theta = (1 + \cos 2\theta)/2$, (Kreyszig, 2006).

Since Eq. 2.87 only gives the expression for the undisturbed potential, it is necessary to find additional terms to represent the disturbance due to the presence of the cylinder. The total potential ϕ_{tot} must satisfy the kinematic body boundary condition that was given in Eq. 2.4, reproduced in Eq. 2.88.

$$\frac{\partial\phi_{\text{tot}}}{\partial r} = 0 \quad \text{at} \quad r = a \tag{2.88}$$

In addition to the condition in Eq. 2.4, ϕ_{tot} must fulfill a far-field requirement which says that the additional terms in ϕ_{tot} compared to the undisturbed ϕ must diminish as r increases. In the absence of the unknown real expression for ϕ_{tot}, one can instead use Eq. 2.87 to find an approximation valid at $z = 0$, like the one given by Manners and Rainey (1992), reproduced in Eq. 2.89.

$$\begin{aligned} \phi_{\text{tot}} &= \phi_0 + D_{001}z + \frac{1}{4}D_{002}(2z^2 - r^2 + 2a^2\ln r) \\ &\quad + (D_{100} + D_{101}z)(r + \frac{a^2}{r})\cos\theta \\ &\quad + (D_{010} + D_{011}z)(r + \frac{a^2}{r})\sin\theta \\ &\quad + \frac{1}{4}(2D_{200} + D_{002})(r^2 + \frac{a^4}{r^2})\cos 2\theta \\ &\quad + \frac{1}{2}D_{110}(r^2 + \frac{a^4}{r^2})\sin 2\theta \end{aligned} \tag{2.89}$$

It is noted that since the approximation in Eq. 2.89 only contains terms up to second order in z, it inherits the characteristics of a Taylor series expansion around $z = 0$. This

combined with the radially decaying disturbance and the kinematic body boundary condition in Eq. 2.4 are features that legitimizes this approximation.

The reason for the foregoing derivation has been to establish an expression for the forces acting on the cylinder. The total integrated force in the x-direction is given by Faltinsen et al. (1995):

$$F_x = -a \int_0^{2\pi} \cos\theta d\theta \int_{-d}^{\zeta} p(a,\theta,z,t) dz = \int_{-d}^{\zeta} F'_x dz \tag{2.90}$$

where F'_x is the differential force which gives the force distribution along the z-axis, defined by

$$F'_x = -a \int_0^{2\pi} p \cos\theta d\theta \tag{2.91}$$

The Bernoulli equation for unsteady potential flow is used to express the pressure p in terms of the potential.

$$-p = \rho \frac{\partial \phi}{\partial t} + \frac{1}{2}\rho \left|\nabla\phi\right|^2 + \rho g z \tag{2.92}$$

The last term on the right hand side of Eq. 2.92 is the hydrostatic pressure, and will not be examined further in the derivation of the forces, hence it will be omitted. The second term is the dynamic pressure. The velocity potential gradient can be written out on the following form, using polar coordinates:

$$\left|\nabla\phi\right|^2 = \left(\frac{\partial\phi}{\partial x}\right)^2 + \left(\frac{\partial\phi}{\partial y}\right)^2 + \left(\frac{\partial\phi}{\partial z}\right)^2 = \left(\frac{\partial\phi}{\partial r}\right)^2 + \left(\frac{1}{r}\frac{\partial\phi}{\partial\theta}\right)^2 + \left(\frac{\partial\phi}{\partial z}\right)^2 \tag{2.93}$$

In accordance with Eq. 2.90, we want the pressure evaluated at the cylinder surface $r = a$. Thus, the first term on the right hand side of Eq. 2.93 must be zero according to the kinematic body boundary condition in Eq. 2.4.

Going back to the differential force in Eq. 2.91, it is convenient to rewrite it into a more manageable form, separating the three pressure terms emerging from Eq. 2.92 and Eq. 2.93, and using the total potential from Eq. 2.89:

$$F'_x = \rho a I_1 + \frac{1}{2}\rho a (I_{21} + I_{22}) \tag{2.94}$$

where

$$\begin{gathered} I_1 = \int_0^{2\pi} \frac{\partial\phi_{\text{tot}}}{\partial t} \cos\theta d\theta, \quad I_{21} = \int_0^{2\pi} \left(\frac{1}{a}\frac{\partial\phi_{\text{tot}}}{\partial\theta}\right)^2 \cos\theta d\theta \\ \text{and} \quad I_{22} = \int_0^{2\pi} \left(\frac{\partial\phi_{\text{tot}}}{\partial z}\right)^2 \cos\theta d\theta \end{gathered} \tag{2.95}$$

in accordance with Manners and Rainey (1992).

To evaluate Eq. 2.94 at $z = 0$ and $r = a$ using the potential from Eq. 2.89, it is useful to see that most of the terms from Eq. 2.89 is evaluated to zero when integrated. Starting with I_1 it can be seen that $\int_0^{2\pi} \cos\theta d\theta = \int_0^{2\pi} \cos\theta \sin\theta d\theta = \int_0^{2\pi} \cos\theta \cos 2\theta d\theta = \int_0^{2\pi} \cos\theta \sin 2\theta d\theta = 0$. The only remaining term is $\int_0^{2\pi} \cos^2\theta d\theta = \pi$, and thus I_1 reduces to:

$$I_1 = 2\pi a \frac{\partial D_{100}}{\partial t} \tag{2.96}$$

The remaining two integrals can be found in the same manner:

$$I_{21} = 2\pi a \left[D_{100} \left(2D_{200} + D_{002} \right) + 2D_{010} D_{110} \right] \tag{2.97}$$

$$I_{22} = 4\pi a D_{001} D_{101} \tag{2.98}$$

Thus

$$\begin{aligned} F'_x &= 2\pi\rho a^2 \left[\frac{\partial D_{100}}{\partial t} + D_{100} \left(D_{200} + \frac{1}{2} D_{002} \right) + D_{010} D_{110} + D_{001} D_{101} \right] \\ &= 2\pi\rho a^2 \left(\frac{\partial u}{\partial t} + u\frac{\partial u}{\partial x} + v\frac{\partial u}{\partial y} + w\frac{\partial u}{\partial z} + \frac{u}{2}\frac{\partial w}{\partial z} \right) \end{aligned} \tag{2.99}$$

using the definition of velocity potential derivatives given in Eq. 2.85. The surprising result here is that besides the unsteady and convective acceleration, there appears an additional term, namely $\frac{u}{2}\frac{\partial w}{\partial z}$. This term is called the axial divergence correction, and its origin and implications will be discussed in Sec. 2.4.2 below.

Rainey (1989) also describes the the forces that must exist at the ends of a submerged cylinder. In the case of a bottom-fixed cylinder piercing the surface, this force at the surface intersection is given as

$$F_{x,SI} = -\frac{1}{2}\rho\pi a^2 \frac{\partial \zeta}{\partial x} u^2 \tag{2.100}$$

This is a point load which first arises at the third order of wave steepness. It is also known as the oblique slam force. If the first-order wave theory is employed, Eq. 2.100 reduces to

$$F_{x,SI} \approx -\frac{1}{8}\pi\rho g k^2 a^2 \zeta^3 \cos 3\omega t \tag{2.101}$$

This force is eight times smaller that the corresponding force given by FNV theory. The combined results of the derivations are presented and discussed below.

2.4.2 Results

The distributed force representing the inertia component of the Morison Equation in Eq. 2.1 was derived in Eq. 2.99 using pressure integration. This force is reproduced below.

$$F_{x,I} = \int_{-d}^{\zeta^{(1)}} 2\pi\rho a^2 \left(\frac{\partial u}{\partial t} + u\frac{\partial u}{\partial x} + v\frac{\partial u}{\partial y} + w\frac{\partial u}{\partial z} \right) dz \tag{2.102}$$

In Eq. 2.102 there has been a couple of changes from the Morison inertia component. The spatial velocity derivatives are taken into account, and thus the total water acceleration is included, both the unsteady and the convective. The integration is extended to the first order instantaneous free surface, by employing some form of stretching. To be comparable to the Morison inertia term, Eq. 2.102 assumes an added mass coefficient of $C_m = 2$.

Apart from the Morison inertia term, Eq. 2.99 showed the appearance of an additional force called the axial divergence force, given in Eq. 2.103.

$$F_{x,AD} = \int_{-d}^{\zeta^{(1)}} \pi\rho a^2 u \frac{\partial w}{\partial z} dz \tag{2.103}$$

This force can be seen as the rate of change of added mass along the cylinder axis. It is the product of the transverse fluid velocity with the longitudinal velocity gradient, and should be added to the water particle acceleration when computing the added-mass component of the force (Manners and Rainey, 1992).

Lastly, the third order surface intersection force point load is given below.

$$F_{x,SI} = -\frac{1}{2}\rho\pi a^2 \frac{\partial \zeta^{(1)}}{\partial x} u^2 \tag{2.104}$$

The velocity components at the mean surface is used when finding the value of Eq. 2.104.

For easier implementation in computer code, the three components will be written on matrix form incorporating the forces in all three directions, as they were originally given by Rainey (1989). Eq. 2.105 gives the distributed differential load, consisting of both the inertia term and the axial divergence term.

$$\mathbf{F}' = \rho c \boldsymbol{a} + \mathbf{M}\left[\mathbf{a} + (\boldsymbol{\ell} \cdot \mathbf{V}\boldsymbol{\ell})\boldsymbol{v}\right] \tag{2.105}$$

c in Eq. 2.105 represents the cross-sectional area of the cylinder, $\boldsymbol{a}$ is the fluid acceleration vector (with both unsteady and convective terms), $\mathbf{M}$ is the two-dimensional diagonal added-mass matrix, $\mathbf{V}$ is the velocity gradient matrix, $\boldsymbol{v}$ is the fluid velocity vector, and $\boldsymbol{\ell}$ is a unit vector along the cylinder axis pointing in the positive z-direction, $\boldsymbol{\ell} = [0, 0, 1]^T$. Written out and integrated, Eq. 2.105 gives Eq. 2.102 and Eq. 2.103 combined. The first term of Eq. 2.105 is known as the Froude-Krylov force, and the second term is the diffraction force with the axial divergence correction. The point load is given by Eq. 2.106, and consists of the surface intersection force previously discussed.

$$\mathbf{F} = \frac{1}{2}\tan\alpha\left[(\boldsymbol{t} \cdot \boldsymbol{v})\mathbf{M}\boldsymbol{v}\right] \tag{2.106}$$

$\boldsymbol{t}$ is a unit vector normal to the cylinder axis, pointing out of the fluid, and $\tan\alpha$ represents the wave slope previously given by the wave elevation derivative in Eq. 2.104.

2.5 Nonlinear Wave Motion

Recent research concerning the description of extreme waves states that for a wave model to be effective, it must incorporate both unsteadiness, directionality and nonlinearity of the waves (Tromans et al., 2006). Nonlinear wave motion models exist both as empirical models and analytical models in closed form. In particular, Cnoidal waves represents nonlinear waves with dispersion in relatively shallow water. It is based on a perturbation of the non-dimensional wave steepness parameter kA, as well as the non-dimensional wave height over wave length parameter kh (Myrhaug, 2006). Cnoidal waves contain Solitary waves and sinusoidal waves, where the wave elevation for Solitary waves is given by

$$\zeta = \frac{A}{\cosh^2\left[\frac{\sqrt{3}}{2}\sqrt{\frac{A}{h^3}}(x - c_w t)\right]} \tag{2.107}$$

where c_w is the wave velocity given by

$$c_w = \sqrt{g(h + A)} \tag{2.108}$$

Qualitatively, Cnoidal waves are symmetric with respect to a vertical axis through the wave crest, and can therefore not describe nonlinear waves with asymmetry with respect to this axis. The wave crest is higher for Cnoidal waves than for linear waves, and the wave trough is correspondingly shallower, in accordance with observations of waves in shallow water (Dean and Dalrymple, 1991).

The validity for different wave theories is shown in Fig. 2.5. Stokes 5^{th} order wave

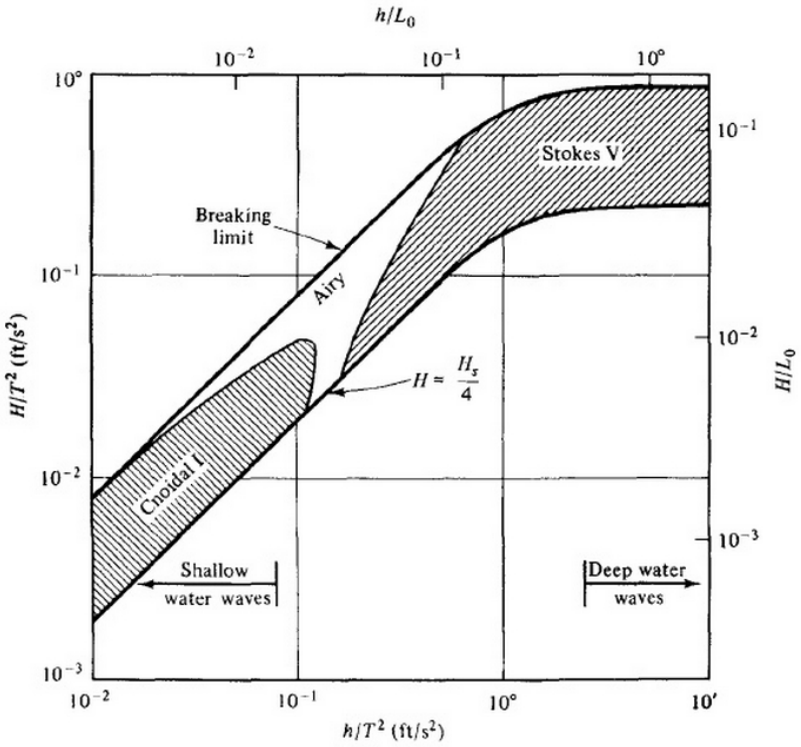

Figure 2.5: *Validity of different wave motion models with respect to wave height and water depth relative to the wave period (Dean and Dalrymple, 1991).*

theory is applicable for deep water, linear wave theory (Airy theory) for intermediate water, and Cnoidal waves for shallow water. It will be seen in later chapters that the sea states used for analyzing a wind turbine in shallow water and extreme waves might legitimize the use of Cnoidal waves according to Fig. 2.5.

Fully nonlinear state of the art wave models exist in many variations. For use together with FNV and Rainey forcing, Tromans et al. (2006) recommends work done by Bateman et al. (2001) & (2003), which provide a efficient wave model with a wave potential that is time marched using a nonlinear free surface boundary condition coupled with a Taylor expansion of the Dirichlet-Neumann operator. In following chapters, the force models will be implemented without a nonlinear wave model, partly because of the tediousness of the implementation, and partly to maintain the focus of the thesis to the study of higher order forcing effects.

2.6 Nonlinear Structural Response

The structure might hold nonlinearities in both material and geometry, of which the relation to the structural response of the wind turbine in storm condition has to be

identified. Material nonlinearity is associated with inelastic behavior of parts of the wind turbine structure, while geometric nonlinearity is associated with resisting forces due to change in geometry, and effects due to curvature. The stiffness matrix of the structure is the combined elastic and geometric stiffness in Eq. 2.109.

$$\mathbf{k} = \mathbf{k_E} + \mathbf{k_G} \tag{2.109}$$

An example of the effect of change in geometry on the structure stiffness is shown for a beam with supported ends in Fig. 2.6. The geometric stiffness arises by including second order strains, as shown below.

$$\epsilon(x, y) = \frac{\partial v_x}{\partial x} - y\frac{\partial^2 v_y}{\partial x^2} + \frac{1}{2}\left(\frac{\partial v_y}{\partial x}\right)^2 \tag{2.110}$$

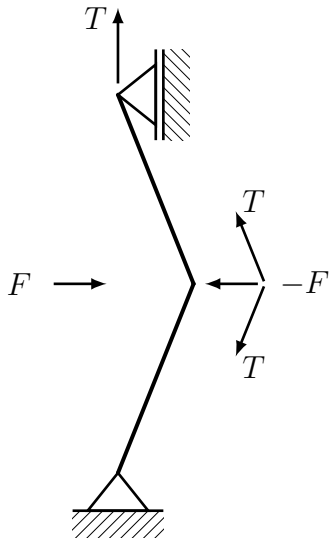

Figure 2.6: *The figure shows the resisting forces due to change in geometry. The geometric element stiffness matrix is dependent on the element axial force and the element length, as illustrated by this two-element structure.*

The investigation of nonlinearities in material and geometry will not be carried out in this thesis, and is saved for future work.

Chapter 3

Software Implementation

The FAST (Fatigue, Aerodynamics, Structures and Turbulence) code is a computer-aided engineering tool for horizontal axis wind turbines, developed by The National Renewable Energy Laboratory (NREL) in the USA. It was originally intended for the analysis of onshore wind turbines, but offshore capabilities has later been added. Its free and open-source nature is the reason why FAST has been chosen as the primary analysis tool for this thesis. Additionally, a reference model of a 5MW monopile offshore wind turbine is provided by NREL, ready to be analyzed by FAST. Thus the task of building a model has been reduced to the task of modifying an existing reference model.

FAST is in continuous development, and a new version (v.8) has just been released at the time of writing this thesis. It features a new code architecture and presumably an improved way of modularizing its components into separate aerodynamic and hydrodynamic modules (Jonkman and Jonkman, 2013). It is however poorly documented, and it was therefore decided to use the better-documented old version of the code (v.7). The FAST user's guide (Jonkman and Buhl Jr., 2005), which is also its official theory manual, is based on an even earlier version of the code, but an addendum was released to cover the changes made to v.7 (Jonkman, 2008).

Even though FAST is intended to run on Windows machines, a patching and recompilation of the source code was performed to make the software run on Linux operating systems. FAST has no user interface, and is solely based on input files for specifying model properties and environmental conditions. The program itself is executed from the terminal, and output files are created according to the user's specifications. FAST is capable of performing both a time marching analysis in the time domain, and a linearization analysis in the frequency domain. However, at this stage in the code development, the last option is not valid for the inclusion of hydrodynamic loads. If a frequency domain analysis is desired incorporating the effects of wave loads, it is therefore necessary to do a discrete Fourier transform of the time series.

Sec. 3.1 will outline the theoretical foundation for the architecture of the FAST code and the components of the wind turbine model. The implementation of the force models as they were presented in the previous chapter is described in Sec. 3.2. A comparison between these and the linear forcing is done in Sec. 3.3 for the case of regular waves.

3.1 Theoretical Foundation

FAST is not well documented and lacks a usable theory manual. The code itself is however readable and extensively commented. One of the creators of FAST, Jason Jonkman, also provided his personal notes roughly describing the theoretical foundation of FAST. Those notes, together with the FAST source code and the user's guide (Jonkman and Buhl Jr., 2005) form the basis of the following survey.

3.1.1 Model Description

A 3-bladed wind turbine model in FAST consist of 24 degrees of freedom (DOFs). Since FAST is made to handle floating offshore wind turbines, six of those DOFs are the rigid body translations (surge, sway, heave) and rotations (roll, pitch, yaw) for the floating support platform. These are fixed and therefore not applicable for the monopile offshore wind turbine with a stiff foundation. The next four DOFs are the first and second mode shapes of the flexible tower, in the fore-aft and side-side direction, respectively. The remaining DOFs are related to turbine and blade mechanics.

Much can be said about the properties of the 5MW reference turbine provided by NREL. It is a sophisticated model that is able to account for blade aerodynamics, hub, nacelle and drivetrain properties etc. The focus here will be on the part where the hydrodynamics act, which is the tower of the wind turbine. It is important to know how this part of the model is constructed, to be able to correctly implement the nonlinear hydrodynamic forcing which was derived in the previous chapter. Fig. 3.1 and Fig. 3.2 shows the tower model with the orientation of the axes and the respective DOFs and length scales, and Fig. 3.3 illustrates the two tower mode shapes.

Figure 3.1: *The axes orientation of the tower support at mudline (Jonkman and Buhl Jr., 2005).*

The properties of the tower depends on the type of support structure to carry the rotor-nacelle assembly, and the support structure will depend on the specific instal-

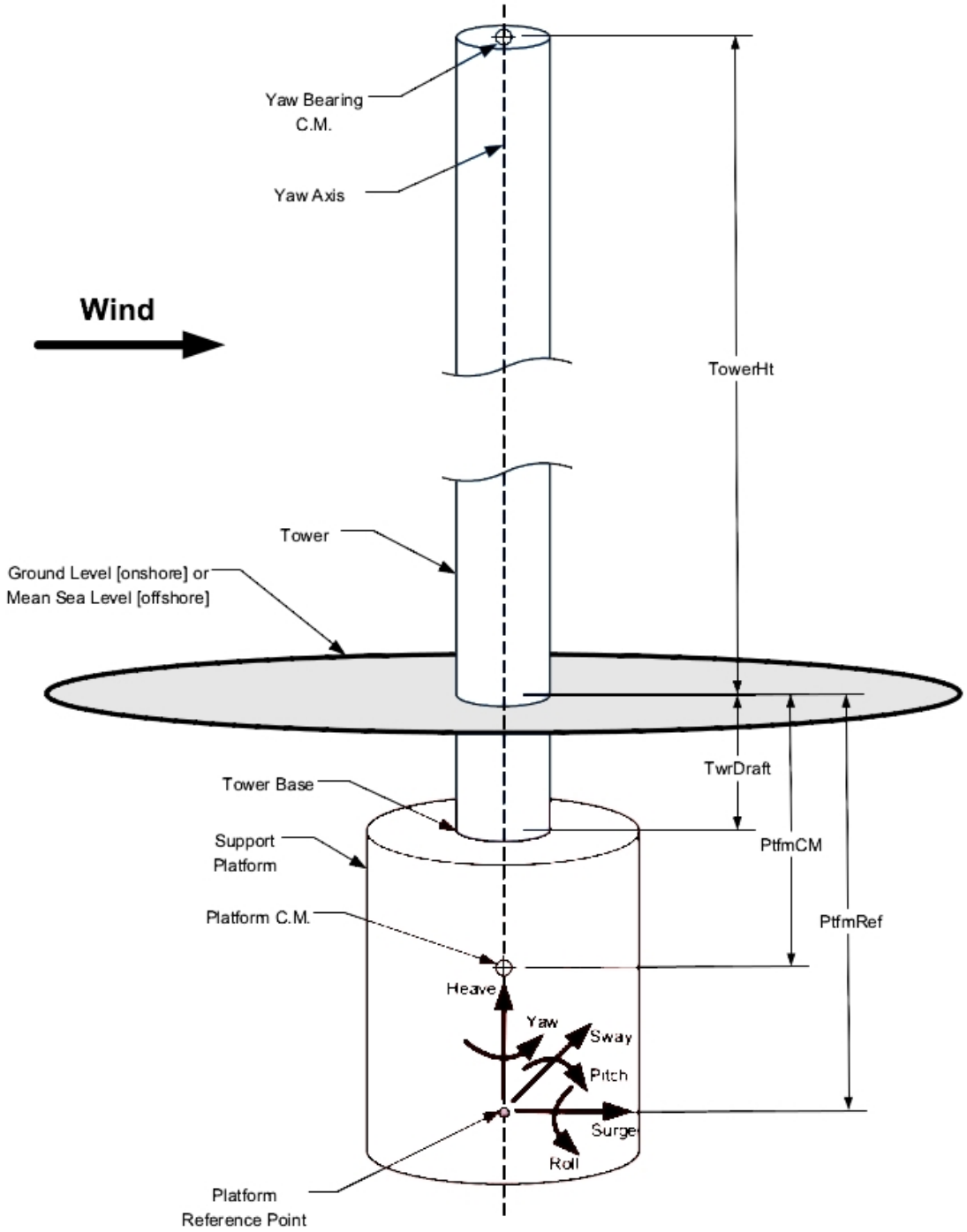

Figure 3.2: *The various length scales of the tower and support platform (Jonkman and Buhl Jr., 2005).*

lation site and in particular the properties of the soil at that place (Jonkman et al., 2009). The model adapted to this thesis is a bottom-fixed monopile with fixed DOFs at the sea bed, which is a configuration representing infinite soil stiffness, and without the inclusion of a support platform. Varying soil stiffness is however obtained by including a massless support platform, and specifying the hydrodynamic stiffness of the platform in accordance with the desired soil stiffness.

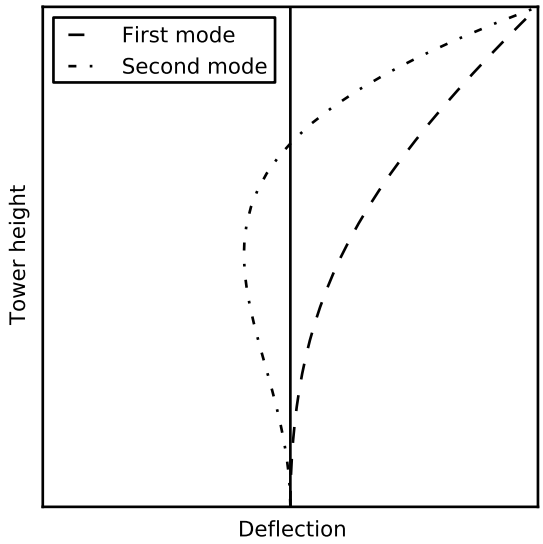

Figure 3.3: *Illustration of the first and second mode shapes of the flexible tower, using the original configuration of the NREL 5MW offshore turbine reference model. The axes are obscured for the figure to be appreciated qualitatively.*

The base diameter of the tower is $6m$ with a thickness of $0.027m$. The top diameter is $3.87m$ with a thickness of $0.019m$. Young's modulus is taken to be $210GPa$, and the shear modulus is taken to be $80.8GPa$. The effective density of the steel is set at $8,500kg/m^3$. The resulting overall tower mass is $347,460kg$ and is centered at $58.234m$ along the tower centerline above mudline, which follows directly from the overall tower height of $107.6m$ above mudline, for a wave height of $20m$ (denoted by TwrDraft in Fig. 3.2). The only one of these parameters that will be modified in the analysis following this chapter, is the Young's modulus, to examine the effect of varying stiffness along the tower.

It should be noted that throughout this thesis, the massless support platform as it is shown in Fig. 3.2 has no span, and thus it is located at the tower base at mudline. This means that PtfmCM and PtfmRef has the same length as the TwrDraft. Everything above the mudline will henceforth be referred to as the tower, and everything below the mudline will be referred to as the foundation.

3.1.2 Mechanics

The flexible components of the wind turbine model are the tower and the blades. FAST uses the mode shapes of these components, but is not capable of producing them internally by means of a modal analysis. If changes are being made to the reference model, the mode shapes are needed to be calculated externally, and then given as input in the initialization of FAST. This is because FAST uses an assumed-modes approach for its flexible components to calculate modal integrals for its equations of motion. There exists a finite-element program written by NREL, that provides dynamically coupled modes for a beam, which is called BModes (Bir, 2013).

In BModes, tower properties are specified together with the magnitude and alignment of the top mass and the foundation stiffness. The output is given as tower eigen

frequencies and mode shapes in the fore-aft and side-side direction. FAST takes as input the first two mode shapes in each direction, as well as the rigid body support platform motion, if any. Torsional modes are not accounted for, and nonlinearity in neither material or geometry is included.

3.1.3 Hydrodynamics

The way FAST natively calculates wave loads on the wind turbine tower is by using Morison's Equation. The tower is divided into equally spaced elements along its height, with nodes placed in the middle of each element, and the wave loads are calculated at each submerged node, using the wave velocities at the tower centerline. The contributions are summed up over the whole submerged part of the tower. If an element is partly submerged, a coefficient describing the level of submersion is multiplied with the force contribution.

Even though FAST does not natively include higher order forcing as an option, a user defined function has been included in the source code with the possibility of overriding the Morison calculated wave loads. This is the option that has been used when implementing the FNV and Rainey model in FAST. Details of this will be given in Sec. 3.2.

Kinematic stretching is supported by FAST, including Wheeler stretching as presented in Sec.2.2.2. The choice of wave direction is arbitrary, but it is not possible to apply spreading of the waves. Nonlinear waves are not supported, and will not be implemented.

FAST supports both periodic linear regular waves, and stochastic linear irregular waves. In the case of the irregular waves, they are created as a sum of regular wave components using the Pierson-Moskowitz (PM) wave spectrum. The wave spectrum is based on data from the North Atlantic Sea, and is given on the form

$$S(\omega) = \frac{A}{\omega^5} e^{-\frac{B}{\omega^4}} \tag{3.1}$$

where the parameters $A = 0.0081g^2$ and $B = 0.74\left(\frac{g}{U}\right)^4$ are given, with U being the wind velocity taken at $19.5m$ above the sea level (Myrhaug, 2007). Thus, the PM spectrum is only dependent on the wind velocity. The spectrum is plotted in Fig. 3.4 for a wind speed of $20m/s$. The spectrum is one-peaked and has a steep front for low frequencies. In FAST, an inverse discrete Fourier transform is used for the transition from the wave spectrum to the incident wave kinematics. The algorithm used for this operation is the Fast Fourier Transform (FFT), which is given in more detail in Sec. 4.3.

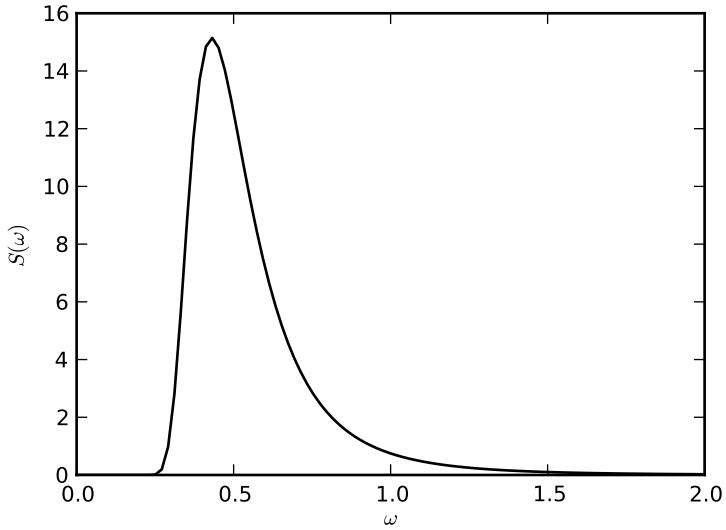

Figure 3.4: *Pierson-Moskowitz spectrum for a wind speed of* $20m/s$.

3.1.4 Operational States

Many operational states and special events can be modeled with FAST (Jonkman and Buhl Jr., 2005). Examples are turbine startup, shutdown due to loss of grid, an idling turbine, a parked turbine etc.

How to model a parked turbine is of particular interest for extreme weather condition, where the wind speed exceeds the cut-out wind speed of the turbine. In the following, a presentation of how to model this with FAST will be given, referring to the relevant input parameter names for completeness.

The rotor speed has to be initialized to zero: $RotSpeed = 0.0$. Pitch control is disabled by setting $PCMode$ equal to 0, and the generator is assured to be turned off by setting the initialization time for the generator higher than the simulation duration: $TimGenOn = 9999.9$. To apply the rotor breaks instantly, $THssBrDp$ is set to 0.0. The blades are fully feathered by setting $BlPitch = 90$ for all the 3 blades. Lastly, the aerodynamic induction has to be disabled, which is obtained by setting $IndModel = None$.

3.2 Implementation of Force Models

The FAST code is open source, and is written in Fortran 90. Because the source code is available, it is possible to do changes to all parts of the program. A dummy placeholder routine for the calculation of hydrodynamic loads on the tower is included in the hydrodynamic module of FAST, and it is called $UserTwrLd$. It can be specified in the FAST input that this user defined routine should override the forces calculated from Morison's Equation. The $UserTwrLd$ routine for the calculation of both the FNV and Rainey forces is given in Appendix A and B, respectively.

Even though this placeholder routine is predefined in the FAST code, the task of implementing the force models has not been straightforward. Since several parameters such as the convective accelerations and wave slope are not natively computed by

FAST, it was needed to write functions to find these parameters, and then pass the values to the $UserTwrLd$ routine. Great care was taken to not interfere with existing functionality when implementing the new ones. A previous master thesis by Rosenlund (2013) has proved useful for the following derivations, as it deals with modification of the FAST source code.

The convective acceleration vector is given in Eq. 3.2 below, used extensively in finding the second and third order FNV components, as well as the first and second order Rainey components.

$$\mathbf{a} = \begin{Bmatrix} \frac{\partial u}{\partial t} + u\frac{\partial u}{\partial x} + v\frac{\partial u}{\partial y} + w\frac{\partial u}{\partial z} \\ \frac{\partial v}{\partial t} + u\frac{\partial v}{\partial x} + v\frac{\partial v}{\partial y} + w\frac{\partial v}{\partial z} \\ \frac{\partial w}{\partial t} + u\frac{\partial w}{\partial x} + v\frac{\partial w}{\partial y} + w\frac{\partial w}{\partial z} \end{Bmatrix} \tag{3.2}$$

The velocity components and the temporal derivatives are already found by FAST. However, the spatial velocity derivatives have to be implemented. These are collected in the wave gradient matrix in Eq. 3.3.

$$\mathbf{V} = \begin{bmatrix} \frac{\partial u}{\partial x} & \frac{\partial u}{\partial y} & \frac{\partial u}{\partial z} \\ \frac{\partial v}{\partial x} & \frac{\partial v}{\partial y} & \frac{\partial v}{\partial z} \\ \frac{\partial w}{\partial x} & \frac{\partial w}{\partial y} & \frac{\partial w}{\partial z} \end{bmatrix} \tag{3.3}$$

FAST implements a plane wave where the the surface elevation is calculated in the 2D plane (x', z'), and thereafter transformed to the three dimensional system (x, y, z). The 2D coordinate system is rotated β degrees to the global, and the transformations between the two follows in Eq. 3.4 below.

$$\begin{aligned} x' &= x\cos\beta + y\sin\beta \\ x &= x'\cos\beta - y'\sin\beta \\ y' &= y\cos\beta - x\sin\beta \\ y &= y'\cos\beta + x'\sin\beta \\ z' &= z \end{aligned} \tag{3.4}$$

The velocities in the two coordinate systems are also related by the following equations (Rosenlund, 2013).

$$\begin{aligned} u &= u'\cos\beta \\ v &= u'\sin\beta \\ w &= w' \end{aligned} \tag{3.5}$$

In shallow water, the first order velocity potential is given by Eq. 3.6 for the case of uniaxial flow in the x'-direction.

$$\phi = \Re\left\{ \frac{igA}{\omega} \frac{\cosh k(z'+h)}{\cosh(kh)} e^{i(\omega t - kx')} \right\} \tag{3.6}$$

The velocities in the 2D coordinate system are simply the spatial derivatives of the potential.

$$\begin{aligned} u' &= \frac{\partial \phi}{\partial x'} = \Re\left\{ \omega A \frac{\cosh k(z'+h)}{\cosh(kh)} e^{i(\omega t - kx')} \right\} \\ w' &= \frac{\partial \phi}{\partial z'} = \Re\left\{ i\omega A \frac{\cosh k(z'+h)}{\cosh(kh)} e^{i(\omega t - kx')} \right\} \end{aligned} \tag{3.7}$$

using the dispersion relation for arbitrary water depth

$$k \tanh kh = \frac{\omega^2}{g} \tag{3.8}$$

The convective accelerations in the 2D coordinate system, $\frac{\partial u'}{\partial x'}$, $\frac{\partial u'}{\partial z'}$, $\frac{\partial w'}{\partial x'}$ and $\frac{\partial w'}{\partial z'}$, are found in a similar manner.

The remaining operation is to transform the accelerations back to the 3D coordinate system (x, y, z). Using the coordinate transformations in Eq. 3.4 and Eq. 3.5, these relations are shown in Eq.3.9 below.

$$\begin{aligned}
\frac{\partial u}{\partial x} &= \frac{\partial u'}{\partial x'} \cos^2 \beta \\
\frac{\partial u}{\partial y} &= \frac{\partial u'}{\partial x'} \cos \beta \sin \beta \\
\frac{\partial u}{\partial z} &= \frac{\partial u'}{\partial z'} \cos \beta \\
\frac{\partial v}{\partial x} &= \frac{\partial u'}{\partial x'} \cos \beta \sin \beta \\
\frac{\partial v}{\partial y} &= \frac{\partial u'}{\partial x'} \sin^2 \beta \\
\frac{\partial v}{\partial z} &= \frac{\partial u'}{\partial z'} \sin \beta \\
\frac{\partial w}{\partial x} &= \frac{\partial w'}{\partial x'} \cos \beta \\
\frac{\partial w}{\partial y} &= \frac{\partial w'}{\partial x'} \sin \beta \\
\frac{\partial w}{\partial z} &= \frac{\partial w'}{\partial z'}
\end{aligned} \tag{3.9}$$

Using the relations in Eq. 3.9 on the convective accelerations in the 2D coordinate system, the convective accelerations for the 3D system as they were collected in the gradient matrix in Eq. 3.3 can be found. The complete expressions are given in Eq. 3.10. Since the velocities are taken at the cylinder centerline $x' = 0$, the exponential terms

all equals 1.

$$\begin{aligned}
\frac{\partial u}{\partial x} &= -ik\omega A\frac{\cosh k(z'+h)}{\sinh kh}\cos^2\beta \\
\frac{\partial u}{\partial y} &= -ik\omega A\frac{\cosh k(z'+h)}{\sinh kh}\cos\beta\sin\beta \\
\frac{\partial u}{\partial z} &= k\omega A\frac{\sinh k(z'+h)}{\sinh kh}\cos\beta \\
\frac{\partial v}{\partial x} &= -ik\omega A\frac{\cosh k(z'+h)}{\sinh kh}\cos\beta\sin\beta \\
\frac{\partial v}{\partial y} &= -ik\omega A\frac{\cosh k(z'+h)}{\sinh kh}\sin^2\beta \\
\frac{\partial v}{\partial z} &= k\omega A\frac{\sinh k(z'+h)}{\sinh kh}\sin\beta \\
\frac{\partial w}{\partial x} &= k\omega A\frac{\sinh k(z'+h)}{\sinh kh}\cos\beta \\
\frac{\partial w}{\partial y} &= k\omega A\frac{\sinh k(z'+h)}{\sinh kh}\sin\beta \\
\frac{\partial w}{\partial z} &= ik\omega A\frac{\cosh k(z'+h)}{\sinh kh}
\end{aligned} \tag{3.10}$$

These are the Fourier coefficients that FAST will use in the Fast Fourier Transform to generate the time series.

The wave slopes are similarly found by differentiation of the first order wave elevation $\zeta' = \Re\{Ae^{i(\omega t - kx')}\}$.

$$\begin{aligned}
\frac{\partial \zeta}{\partial x} &= -ikA\cos\beta \\
\frac{\partial \zeta}{\partial y} &= -ikA\sin\beta
\end{aligned} \tag{3.11}$$

Implicitly, the real parts of Eq. 3.10 and Eq. 3.11 are considered.

3.2.1 FNV

The equations of the FNV model are restated below.

$$F_1 = 2\pi\rho a^2\int_{-d}^{0} u_t dz \tag{3.12}$$

$$F_2 = \pi\rho a^2\int_{-d}^{0}(2ww_x + uu_x)dz + 2\pi\rho a^2 u_t\zeta \tag{3.13}$$

$$F_3^{(\phi)} = \pi\rho a^2\left[\zeta\left(u_{tz}\zeta + 2ww_x + uu_x - \frac{2}{g}u_t w_t\right) - \frac{u_t}{g}(u^2+w^2)\right] \tag{3.14}$$

$$F_3^{(\Psi)} = 4\frac{\pi\rho a}{g}u^2 u_t \tag{3.15}$$

Eq. 3.13 and 3.14 make use of the convective accelerations in Eq. 3.10. In addition, the u_{tz} term has to be established, and is found in a similar manner as the convective accelerations. It is given in Eq. 3.16.

$$\frac{\partial^2 u}{\partial t \partial z} = ik\omega^2 A \frac{\sinh k(z'+h)}{\sinh kh} \cos\beta \tag{3.16}$$

The distributed terms of the FNV equations are implemented as a sum of the forces at each node along the submerged part of the tower, while the point forces are lumped at the position of the free surface, using wave kinematics of the mean surface level $z = 0$. In reality, these forces are also distributed from $z = 0$ to $z = \zeta$. The downside to lumping the forces are that the moments will not be of correct order of magnitude. In FAST, a check is performed to see whether the element in question is partly submerged, in other words if the free surface acts along the element. If this is the case, the point forces are applied to the node of this element, and if not, no contribution is given from these forces.

The equations are similar for flow in the y-direction as they are for the x-direction given above.

3.2.2 Rainey

The equations of the Rainey model are restated below.

$$F_I = \int_{-d}^{0} 2\pi\rho a^2 \left(u_t + uu_x + vu_y + wu_z\right) dz \tag{3.17}$$

$$F_{AD} = \int_{-d}^{0} \pi\rho a^2 u w_z dz \tag{3.18}$$

$$F_{SI} = -\frac{1}{2}\rho\pi a^2 \frac{\partial\zeta}{\partial x} u^2 \tag{3.19}$$

The convective accelerations from Eq. 3.10 appear both in the inertia force in Eq. 3.17 and the axial divergence force in Eq. 3.18, while the wave slope from Eq. 3.11 appears in the surface intersection force in Eq. 3.19. The distributed Rainey forces are here integrated up to the mean surface level. For the surface intersection point load, as similar check of partly submersion is performed, as it was with the FNV point loads. The forces in the y-direction are found in a similar manner as the forces in the x-direction above.

3.3 Comparison of Force Models

Tromans et al. (2006) compared the FNV and Rainey forces to work done by Lighthill in 1979. Lighthill derived forces according to the Morison's inertia load, a force due to the integration of dynamic pressure $-\frac{1}{2}\rho(\nabla\phi)^2$ over the surface of the column, a waterline force and a force due to nonlinear potential.

The first order force of both FNV and Rainey are both equal to the first order inertia force in Morison's Equation. For regular waves, the second order FNV force in Eq. 3.13 is equal to the sum of the Lighthill dynamic force and waterline force. Tromans et al. (2006) shows that for regular waves in infinite water depth, the Rainey

force due to convective accelerations in Eq. 3.17 is equal to the Lighthill waterline force, and the axial divergence force in Eq. 3.18 is equal to the Lighthill dynamic force. Thus, under these conditions, there is agreement between Lighthill, FNV and Rainey on the second order forces. The third order forces are generally not in agreement.

A test case of the wind turbine model subjected to regular waves will be performed, to compare the FNV and Rainey forces to the linear forces from Morison's Equation, as well as a comparison between the forces of different orders of magnitude. Table. 3.1 gives the sea state used in the simulations. Regular waves are used to check the validity of the statements above.

Table 3.1: *Parameters of regular incident waves used to run a test case for force model verification.*

Tower radius at mudline, a	$3m$
Water depth, d	$20m$
Significant wave height, Hs	$6m$
Peak wave period, Tp	$11s$
Wind	None

A comparison is shown in Fig. 3.5 for the mudline shear force, and another one in Fig. 3.6 for the mudline moment. The output is only started at $130s$, after the simulation has stabilized, and is shown for approximately four wave periods. No discernible difference is seen between the Morison forces, FNV forces and Rainey forces in this sea states. That is, the second and third order components are small compared to the first order component. As should be expected, the first order FNV and Rainey forces are equal, since they are both equal to the first order Morison inertia force. No discernible difference can be seen between the second order FNV and Rainey forces, in agreement with the observations by Tromans et al. (2006) stated above. The third order forces and moments are different, with the Rainey components having the biggest impact for this sea state, but the forces are of the same order of magnitude, and have the same orders of harmonics.

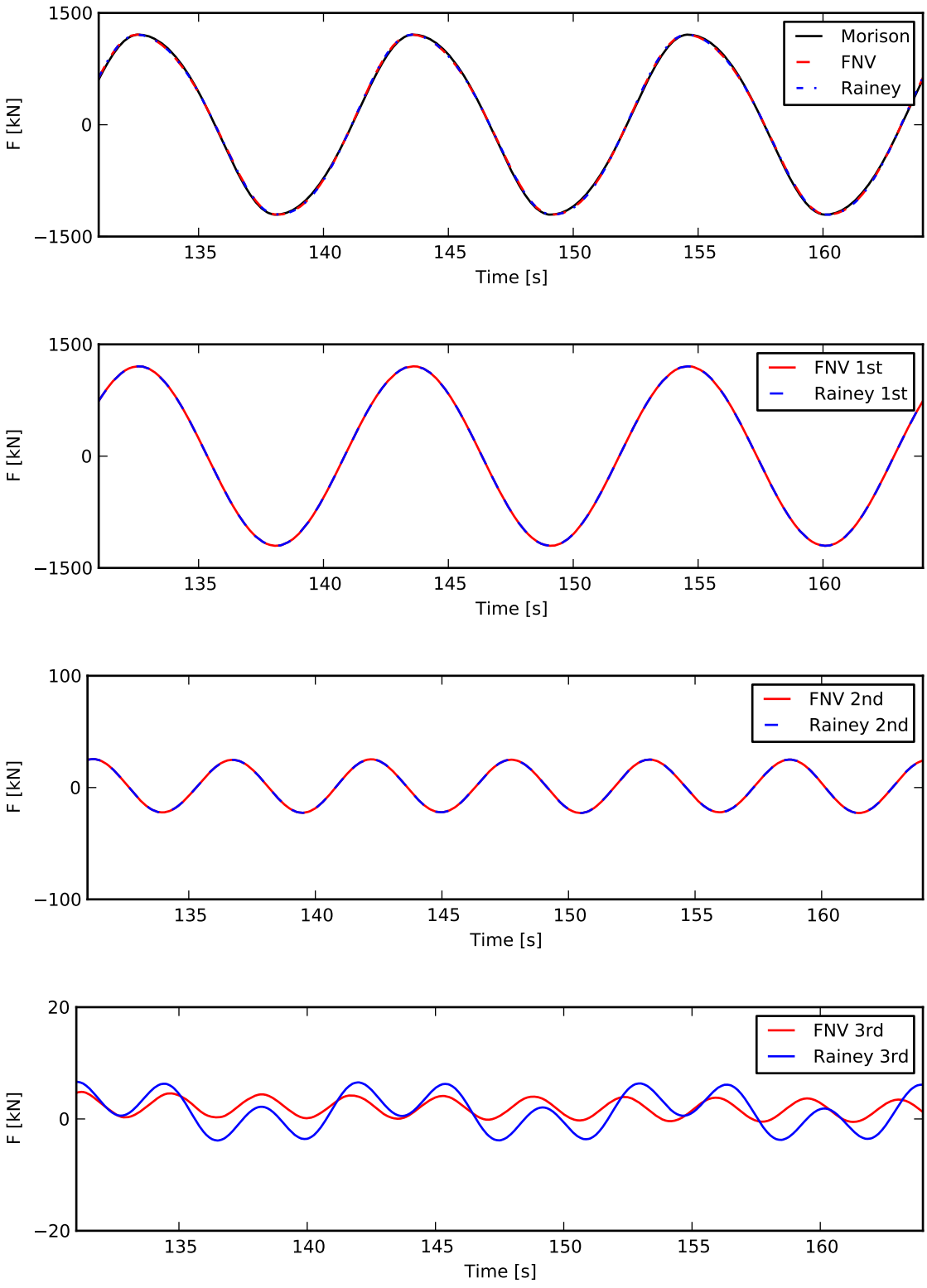

Figure 3.5: *The mudline shear force resulting from the different forcing components.*

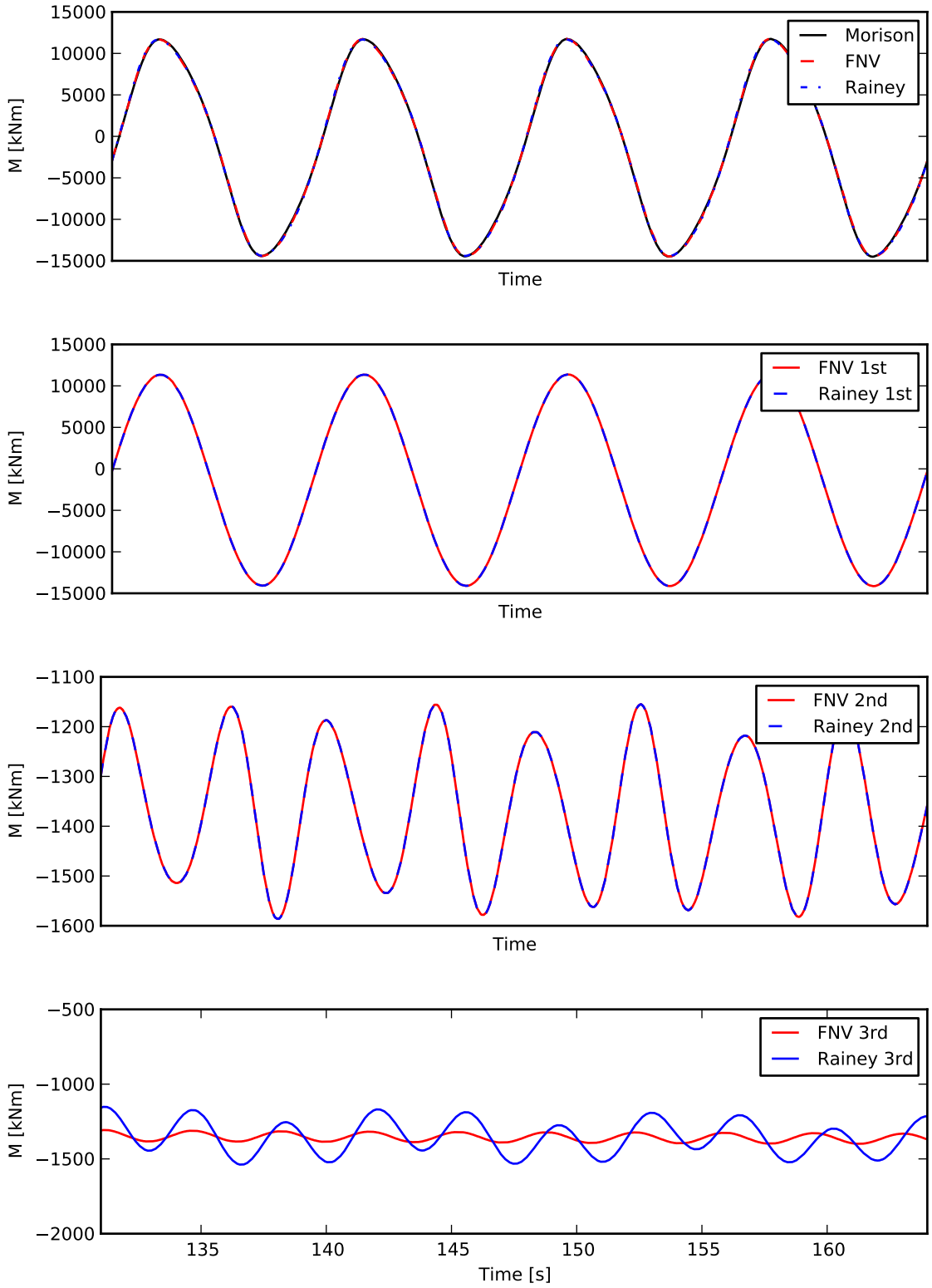

Figure 3.6: *The mudline bending moment resulting from the different forcing components.*

Chapter 4

Dynamic Analysis

This chapter deals with dynamic analysis of a wind turbine model for different operational states and tower configurations. Sec. 4.1 gives the turbine characteristics and Sec. 4.2 gives the environmental conditions used for the analysis. A brief presentation of the discrete Fourier transform is given in Sec. 4.3, and the dynamic analyses are then carried out in Sec. 4.4 through Sec. 4.6 for varying turbine configurations. At last, discussion of results, uncertainties and sources of error are discussed in Chapter 5, together with recommendations for future work.

4.1 Turbine Characteristics

A dynamic analysis of the wind turbine model described in Sec.3.1.1 will be performed. The model is based on the three bladed 5MW reference turbine created by NREL, and it is modified to facilitate the effects of dynamic response that is sought in this section. Fig. 4.1 describes the turbine proportions, and Table 4.1 describes some of the main turbine characteristics (Jonkman et al., 2009). The boundary condition at the seabed

Table 4.1: *Central parameters of the wind turbine, some of which are going to be altered in later sections.*

Rated power	$5MW$
Rotor orientation, configuration	Upwind, 3 blades
Control	Variable speed
Rotor diameter, hub diameter	$126m$, $3m$
Hub height	$90m$
Tower length	$107.6m$
Tower base diameter	$6m$
Tower top diameter	$3.87m$
Sea depth	$20m$
Top mass	$3.5 \times 10^5 kg$
Tower mass	$347,460kg$
Cut-in, rated, cut-out wind speed	$3m/s$, $11.4m/s$, $25m/s$
Cut-in, rated rotor speed	$6.9rpm$, $12.1rpm$

is fixed in Fig. 4.1, but it will later be changed in Sec. 4.5 and 4.6 to account for varying soil stiffness.

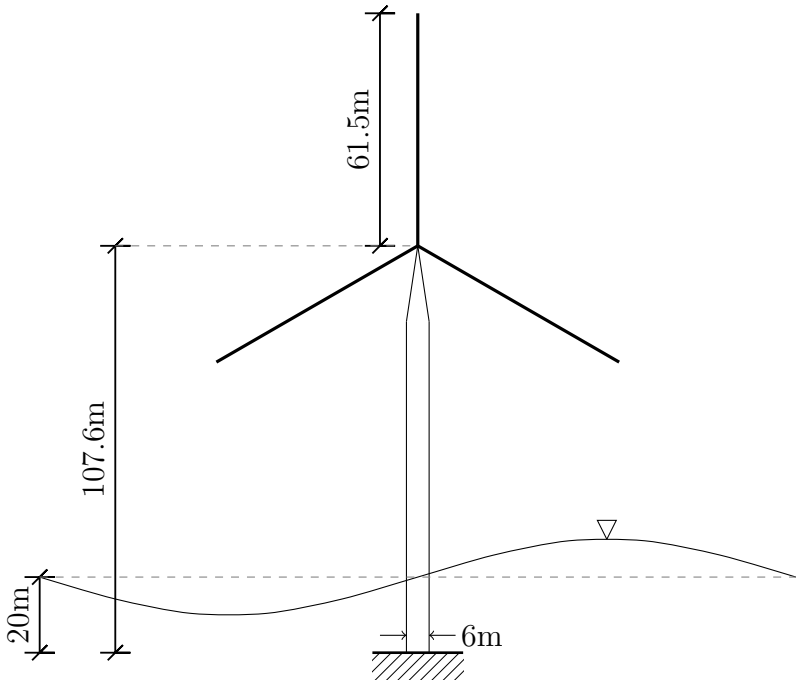

Figure 4.1: *The dimensions of the wind turbine for the case of stiff soil. The total top mass including the nacelle, hub and blades is* $3.5 \times 10^5 kg$.

When modeling the offshore wind turbine, one of the main things to consider is the excitation frequencies, and the most visible source of excitation of the wind turbine is the motion of the rotor (van der Tempel and Molenaar, 2002). The rotational speed of the rotor is related to the excitation frequency, and the wind turbine has to be designed so that its first natural frequency does not coincide with the excitation frequencies. For a three-bladed wind turbine with constant rotational speed, the first excitation frequency is the frequency of the rotor, referred to as 1P. The second is the blade passing frequency, referred to as 3P. These frequencies are illustrated in Fig. 4.2.

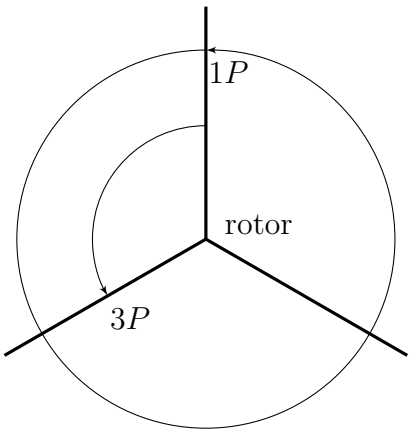

Figure 4.2: *Illustration of the excitation frequencies due to the blade rotations. 1P is the frequency of the rotor rotating one period. 3P is the blade passing frequency at a certain point.*

As can be seen from Table 4.1, the rotor speed operates in the range of $6.9 rpm$ to

12.1rpm. In other words, the first rotational excitation frequency lies in the range of $1P = [0.115, 0.202]Hz$, while the second excitation frequency lies in the range of $3P = [0.345, 0.605]Hz$. This range is plotted in Fig. 4.3, together with a definition of what is meant by a soft-soft, soft-stiff and stiff-stiff structure. If the first eigen frequency

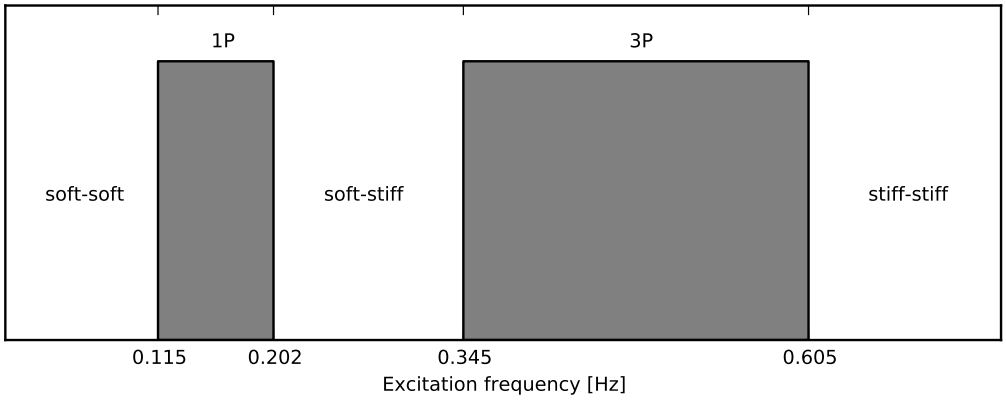

Figure 4.3: *The domains of the first and second excitation frequency from the rotor. To avoid resonant behaviour, either a soft-soft, a soft-stiff or a stiff-stiff wind turbine should be sought.*

of the wind turbine coincides with one of the gray areas in Fig. 4.3, there is the risk of resonant behavior. Thus, the wind turbine could be designed with the first eigen frequency belonging to one of the three non-resonant regions. In consultation with Krokstad (2014) and Jonkman et al. (2009), a first natural frequency of approximately $f_1 = 0.27Hz$ is desired for this particular wind turbine, hence a soft-stiff structure.

4.2 Environmental Conditions

The design of offshore wind turbines in ultimate limit state (ULS) is based on a characteristic load effect with an annual probability of exceedance of less than 0.02, in other words with a return period of at least 50 years, according to DNV (2013). This in contrast to the characteristic load effect with a return period of 100 years for other offshore installations. The wave conditions that will be used in this section is derived using a deterministic design wave method suitable for extreme loading conditions, and will be based on environmental data from the Dogger Bank wind farm, where bottom-fixed wind turbines similar to the one described in this thesis are installed.

In determining a 50-year sea state, previous storm data from the NORA10 hindcast is used. The data was proved by Engebretsen (2012) to be conservative in determining a 50 year sea state, when comparing with the results obtained by the SWAN (Simulating Waves Near Shore) wave model, which is a model based on solving a conservation of wave action equation. The NORA10 data will nevertheless be used as the basis of choosing the sea state used for the following dynamic analysis. The three largest observed storms at the south side of Dogger Bank where the water depth is approximately $20m$, orginating from the north side of Dogger Bank where the water depth is approximately $80m$, is given in Table. 4.2 (Engebretsen, 2012). The direction of wind and wave propagation is approximately the same, and will be assumed equal in the

following calculations. Sea state 1 in Table 4.2 will be used as the dimensioning sea

Table 4.2: *The three largest sea states at the southern point of Dogger Bank from the NORA10 hindcast.*

Hs [m]	Tp [s]	Wind speed [m/s]
10.20	15.98	24.00
8.60	15.03	23.52
8.30	14.45	21.12

state. The wind speed of $24.00m/s$ is close to the cut-off speed given in Table 4.1. Hence, it is purposeful to run the simulations both with a parked and running turbine. Additionally, it is interesting to examine the effects of hydrodynamic loads separately, ie. when the turbine is not influenced by wind loads. The absence of wind in an extreme sea state is not realistic, but will nevertheless be simulated to illuminate the effects of higher order hydrodynamic forcing on the dynamic response of the wind turbine. The three load cases of interest are summarized in Table 4.3. For all the simulations, irregular waves from the Pierson-Moskowitz spectrum is used as defined in Sec. 3.1.3. The wind loads are calculated using the TurbSim software provided by

Table 4.3: *The three load cases that are used in the dynamic response analysis.*

Load case	Hs [m]	Tp [s]	Wind speed [m/s]	Operational state
1	10.20	15.98	24.00	Running turbine
2	10.20	15.98	24.00	Parked turbine
3	10.20	15.98	0	-

NREL. It generates turbulent wind files used as inputs to FAST. The wind speeds in Table 4.3 are defined at hub height, 90m above the sea surface.

4.3 Transformation to the Frequency Domain

Since FAST is only capable of running a time marching simulation when accounting for hydrodynamic loads, a frequency representation of the response has to be created post simulation. Fast Fourier Transform (FFT) is an algorithm to compute the discrete Fourier transform and its inverse (Press et al., 2007). The purpose of Fourier analysis is to convert time to frequency and vice versa. The SciPy extension package for the Python programming language provides a toolbox with functions and methods related to FFT.

The discrete Fourier transform is given in Eq. 4.1 in its general form, accounting for complex numbers.

$$A_k = \sum_{m=0}^{n-1} a_m \exp\left\{-2\pi i \frac{mk}{n}\right\}, \quad k = 0, \ldots, n-1 \tag{4.1}$$

To find the energy A_k at a particular frequency k, the signal in the time domain a_m is spun around a circle and averaged over points along the path. The energy representation used throughout the rest of the thesis is the power spectrum density (PSD), defined by the square of the absolute value of the output: $|A|^2$.

4.4 Stiff Foundation, Flexible Tower

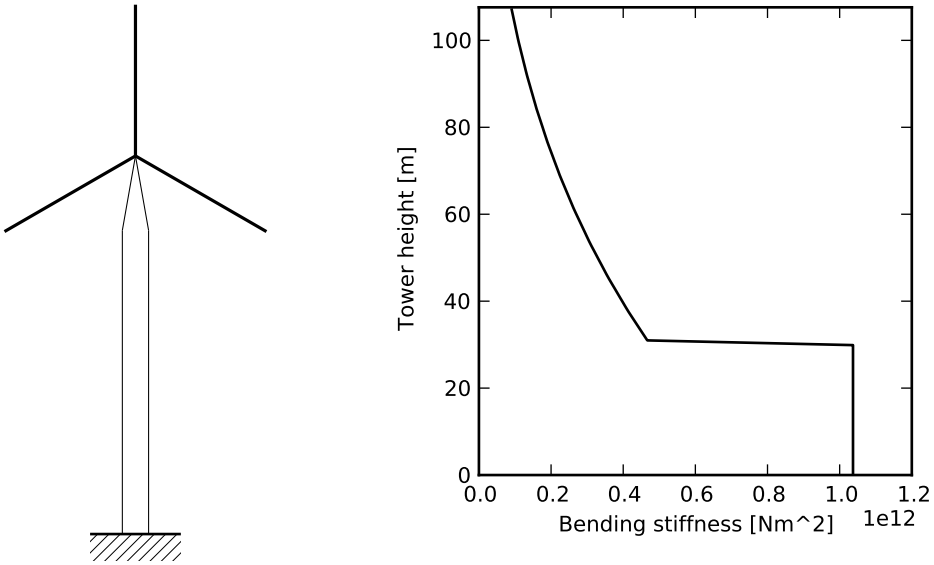

(a) Infinitely large foundation stiffness.

(b) Varying stiffness along the tower.

Figure 4.4: *Soil and tower properties for the case of a stiff foundation and a flexible tower. The stiffness in the fore-aft and side-side direction are equal. The first natural frequency of the wind turbine tower is* $f_1 = 0.27Hz$.

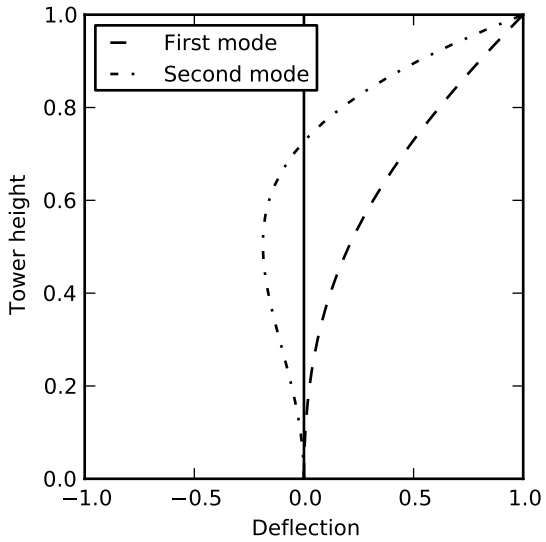

Figure 4.5: *The first and second normalized mode shapes for the stiff foundation and flexible tower configuration.*

Various tower configurations will be examined in this and the following sections. First, the case of a foundation in soil with infinitely large stiffness, together with a flexible tower, will be considered. This is the standard configuration of the NREL

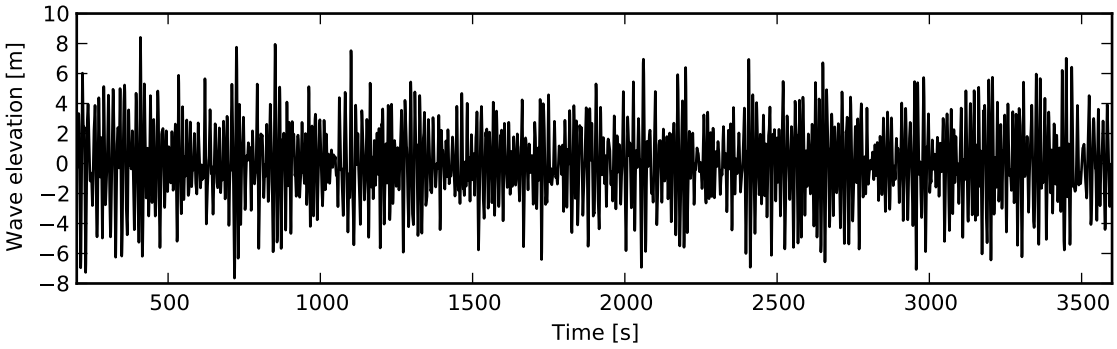

Figure 4.6: *Wave elevation for the whole one hour simulation.*

reference turbine, and it is shown in Fig. 4.4. The first natural frequency is fixed at $f_1 = 0.27Hz$, as will be the case for all the foundation-tower configurations. The normalized first and second mode shapes are shown in Fig. 4.5.

A simulation of one hour is performed for the various loading conditions given in Table 4.3. Regions of large response are then examined closer to evaluate the impact of different force models and foundation-tower configurations.

Fig. 4.6 shows the wave elevation for the whole hour of simulation. The region of largest response was found to be around the 700 second mark. A time series of 100 seconds is shown in Fig. 4.7, together with a time series visualization of the displacement of the top of the turbine, the shear force at mudline and the mudline moment for the case of a running turbine. It is hard to see a difference between the three force models from these plots, in any of the plotted parameters. A zoom in on the region of largest impact of the mudline moment is given in Fig. 4.8, where the higher order contributions from FNV and Rainey moments can be distinguished from the linear forces. The difference is however minor.

In large sea states like the one simulated, the turbine will likely be parked. Fig. 4.9 shows a comparison between the different operational states and loading conditions on the mudline moment. The simulation with no wind generates a moment oscillating around an equilibrium close to zero, as should be expected when the moment is only caused by wave loads. When introducing wind loads, the magnitude of the moment is increased, while the main oscillations still follow the pattern for the case with no wind. The running turbine gives rise to more short time oscillations than the parked turbine, due to the rotor dynamics. The PSD plot reveals that the moment magnitude at the incident wave frequency $1/15.98 = 0.063Hz$ is unaffected by the wind loading.

The higher order force components of FNV and Rainey will excite the wind turbine at higher frequencies than the linear forces. A PSD plot of the three benchmark parameters (top displacement, mudline shear force, mudline moment) is shown in Fig. 4.10 to look for differences in the excitation frequencies. The simulation with no wind loads makes for less noise in the PSD plot, as Fig. 4.9 showed, and thus easier see the hydrodynamic effects isolated.

The moment along the tower is shown in Fig. 4.11 for one wave period. The nine circles along the tower are the sensors where the moment values are measured, and the moment distribution is interpolated between these point.

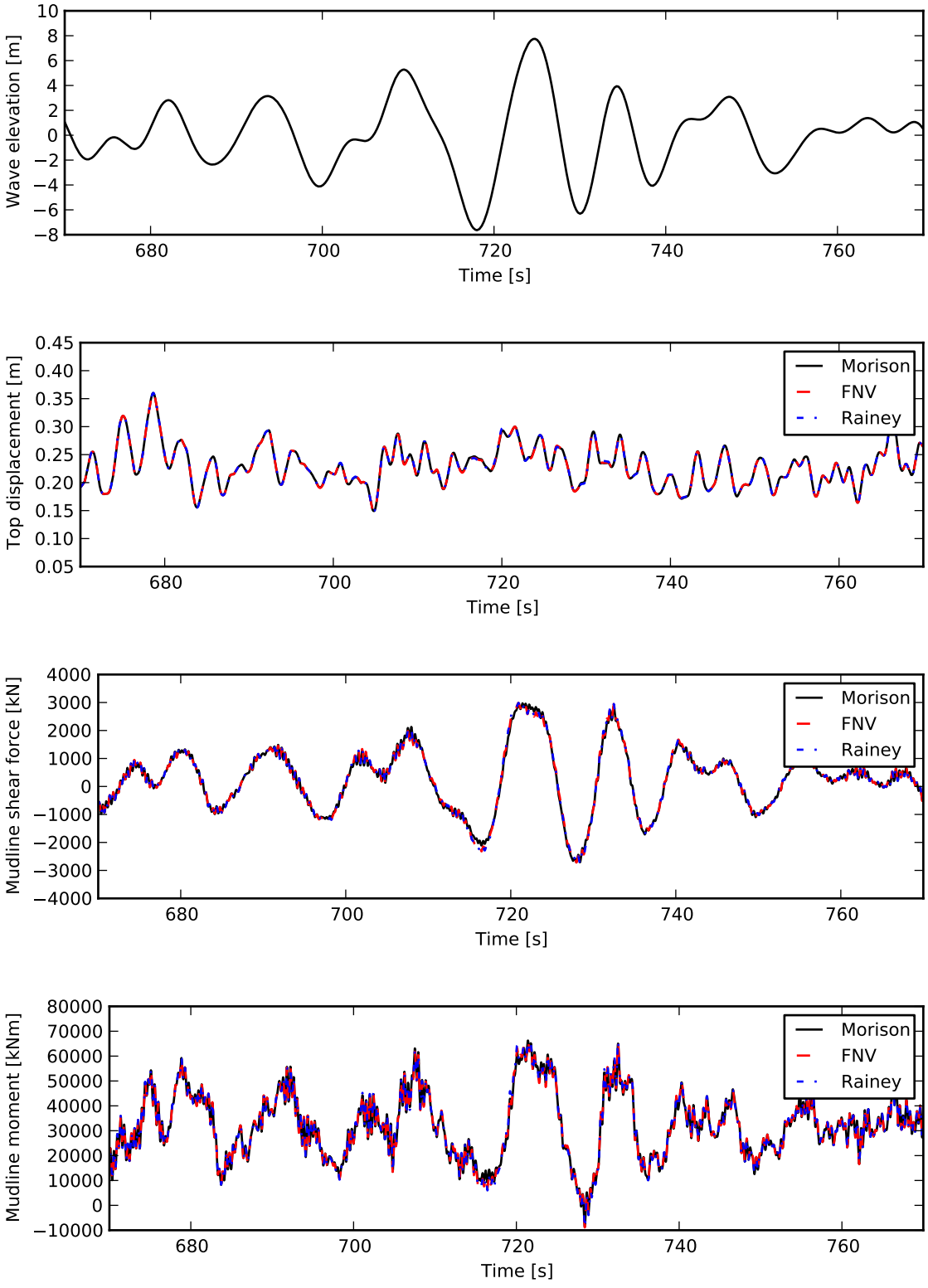

Figure 4.7: *Wave elevation, top displacement, mudline shear force and mudline moment plotted as a time series for a running turbine. A comparison is given between Morison, FNV and Rainey forces.*

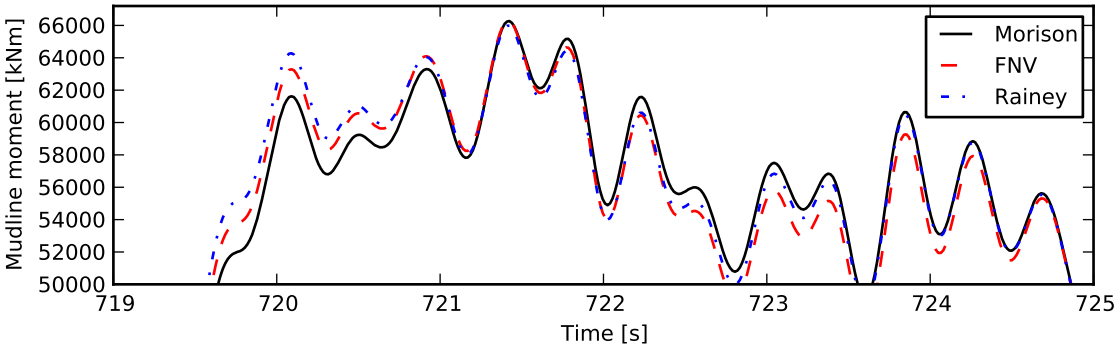

Figure 4.8: *Zoom in on the region of largest impact for the mudline moment.*

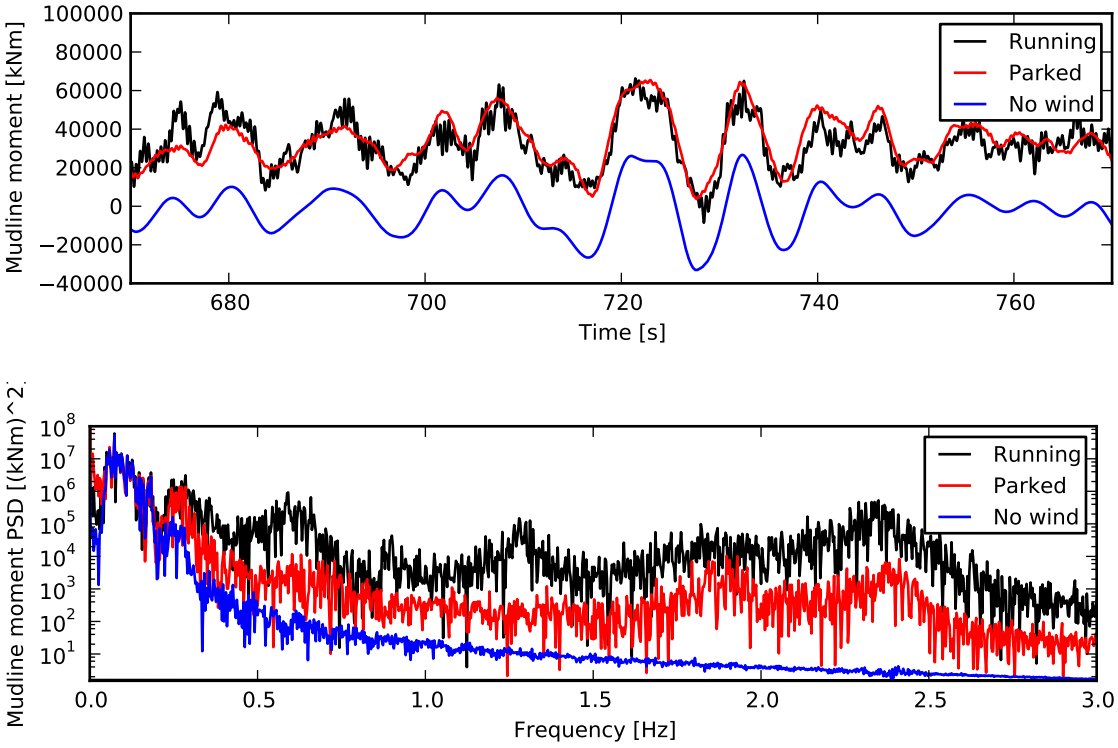

Figure 4.9: *Comparison between different operational states and loading conditions on the mudline moment. The top figure gives a time series representation, and the bottom figure shows a power spectrum density plot of the mudline moment in the frequency domain. Morison forces are used for all the simulations.*

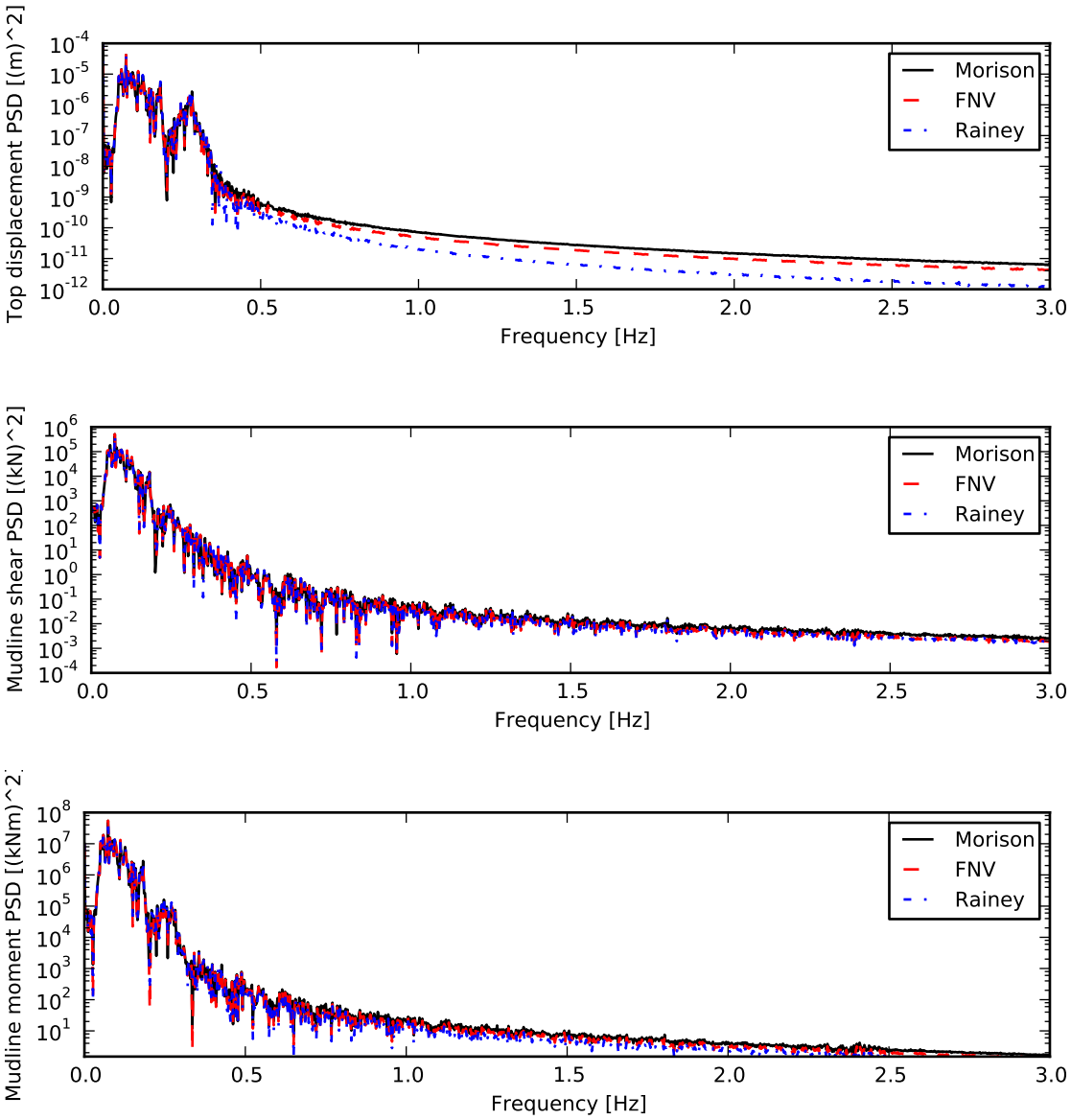

Figure 4.10: *PSD of the top displacement, mudline shear force and mudline moment for the case of no wind.*

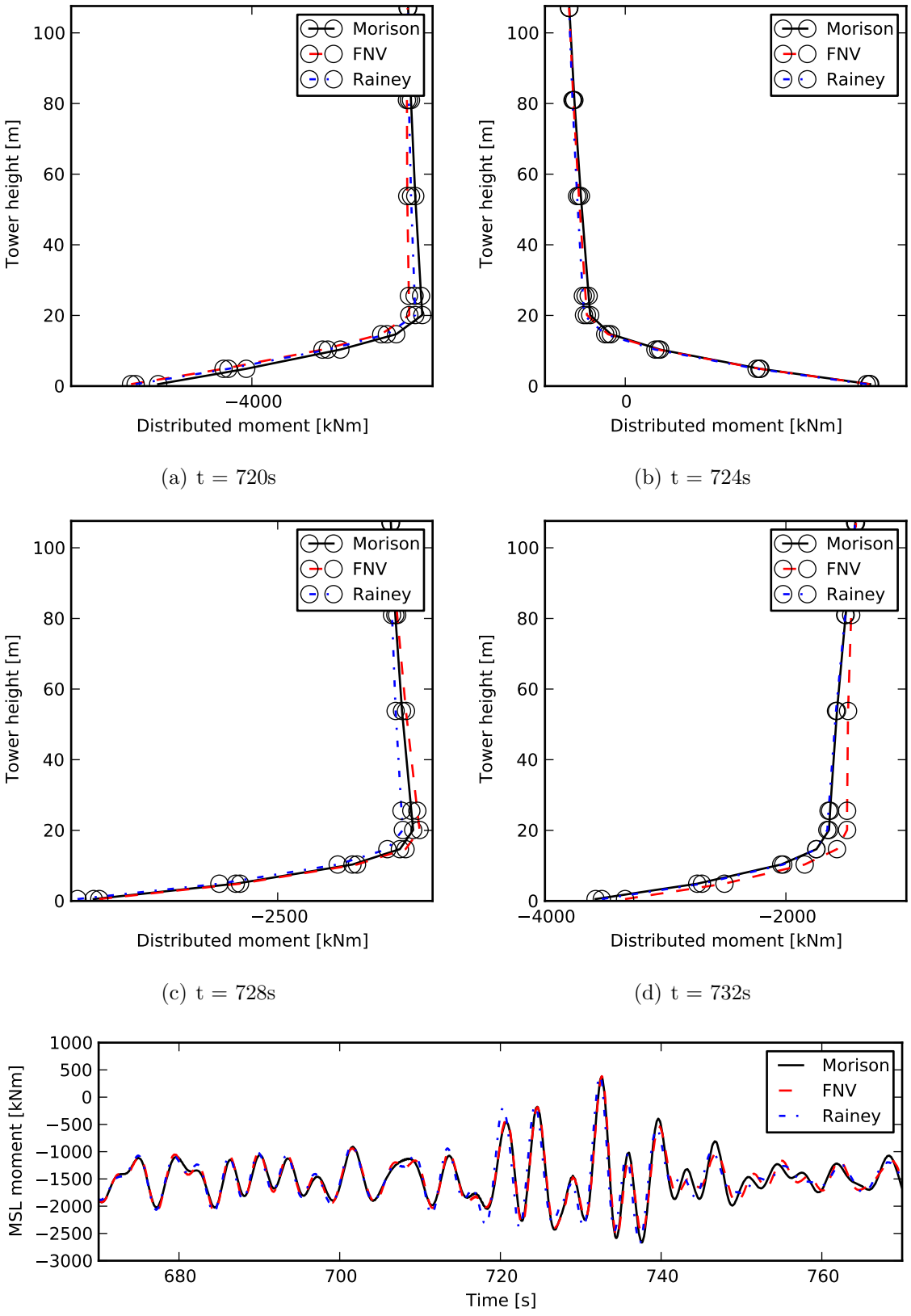

(a) t = 720s

(b) t = 724s

(c) t = 728s

(d) t = 732s

Figure 4.11: *Snapshots of the vertical moment distribution during one wave period. At the bottom, the whole time series for the moment at the mean surface level is plotted.*

4.5 Flexible Foundation, Stiff Tower

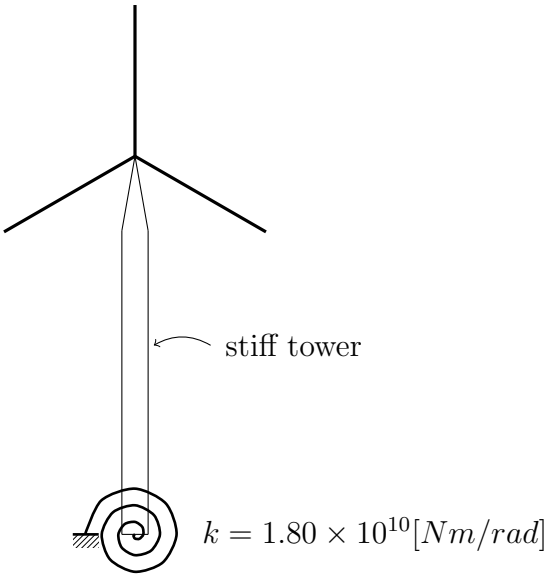

Figure 4.12: *Soil and tower properties for the case of a flexible foundation and a stiff tower. The first natural frequency of the wind turbine tower is* $f_1 = 0.27Hz$.

A flexible foundation due to soil stiffness was modeled by including a massless support platform and subject it to a hydrodynamic stiffness equal to the wanted soil stiffness. The magnitude of the soil stiffness was found by having a stiff tower and varying the soil stiffness until the desired first natural frequency of $f_1 = 0.27Hz$ was obtained. The stiff tower was acquired by using a predefined scaling factor for the stiffness and Young's modulus in one of the input files of FAST. This scaling factor was set to a high number.

Fig. 4.7 shows the time series of the different benchmark parameters for a running turbine, and Fig. 4.14 gives the corresponding PSD series.

A comparison between the present configuration and the previous configuration is given in Fig. 4.15. The top displacement is plotted in both the time and frequency domain for the two configurations, comparing Morison and Rainey forces (omitting FNV forces to keep the plots readable).

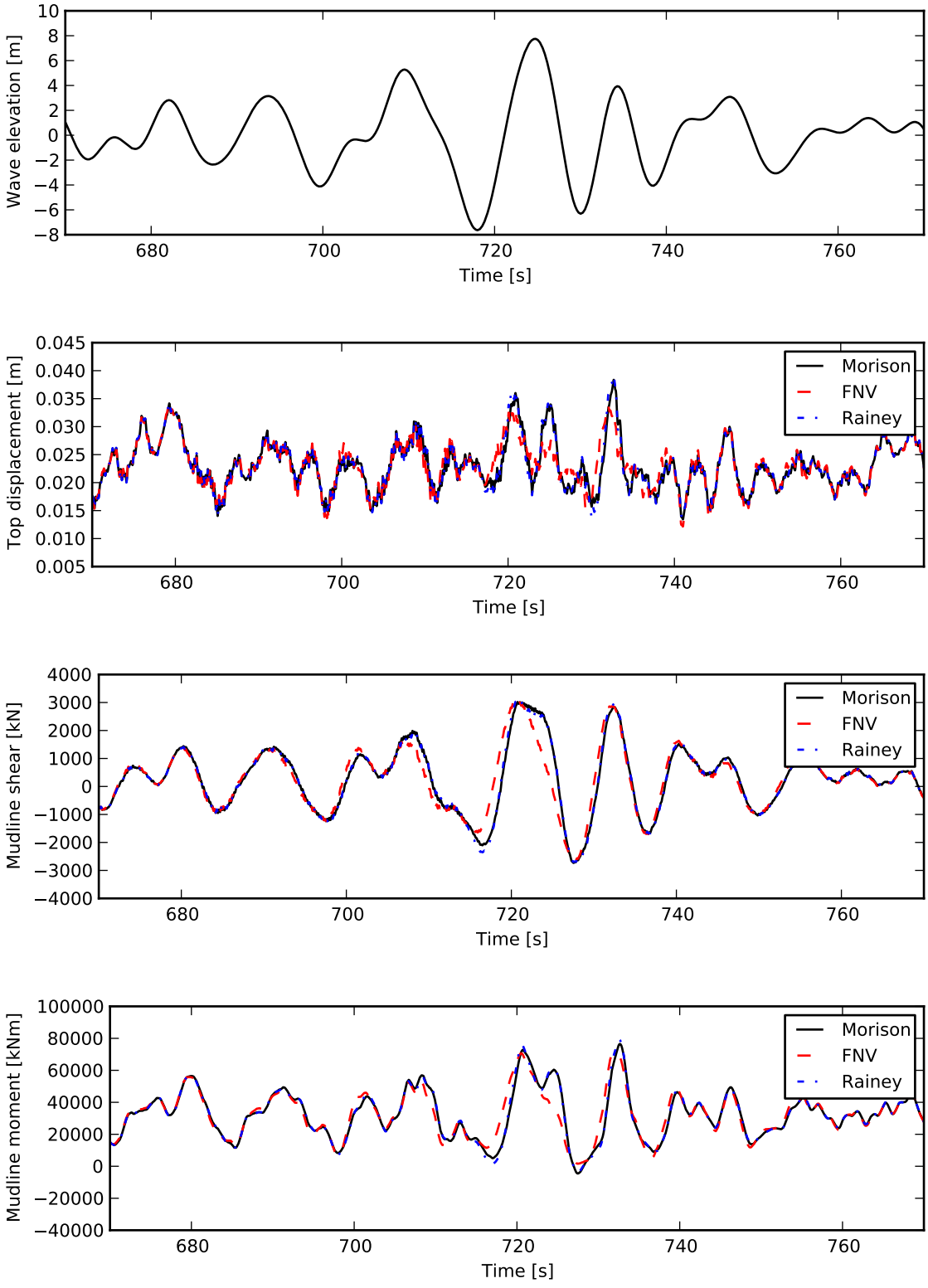

Figure 4.13: *Wave elevation, top displacement, mudline shear force and mudline moment plotted as a time series for a running turbine. A comparison is given between Morison, FNV and Rainey forces.*

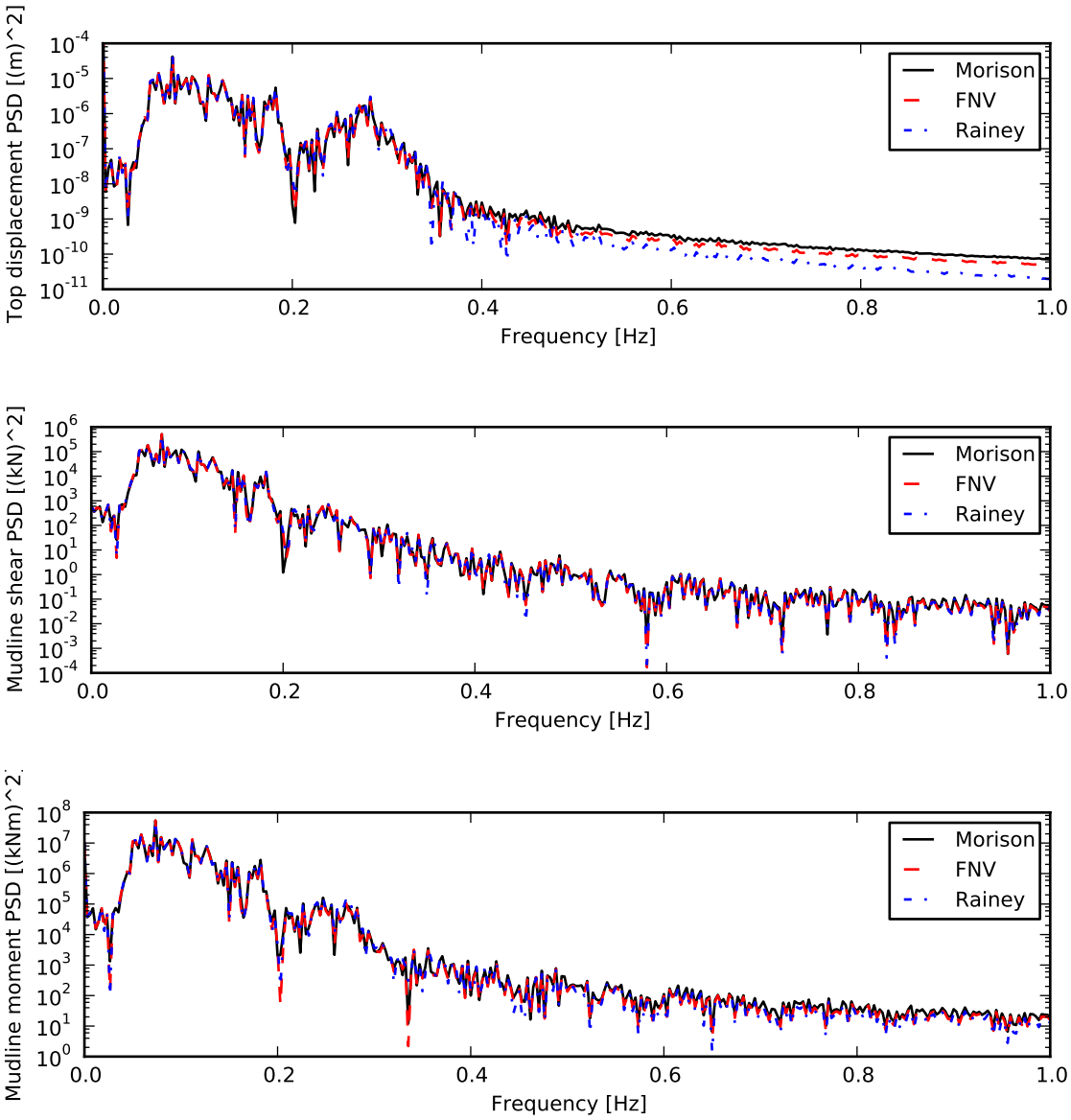

Figure 4.14: *PSD of the top displacement, mudline shear force and mudline moment for the case of no wind.*

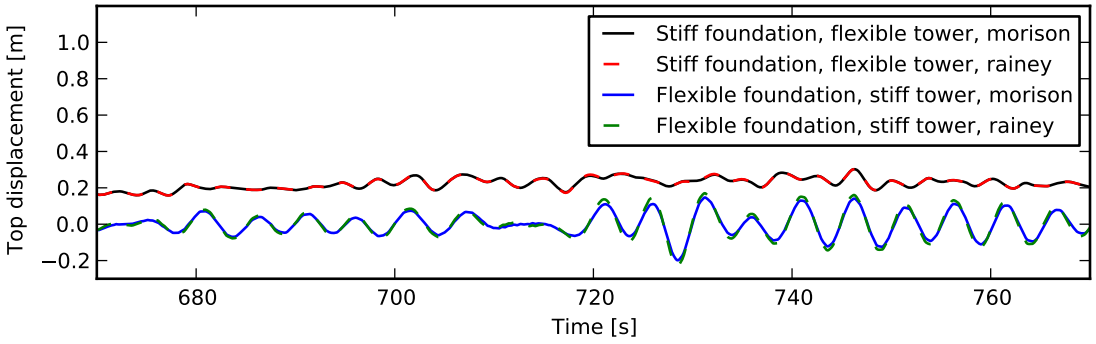

(a) Time series, parked turbine

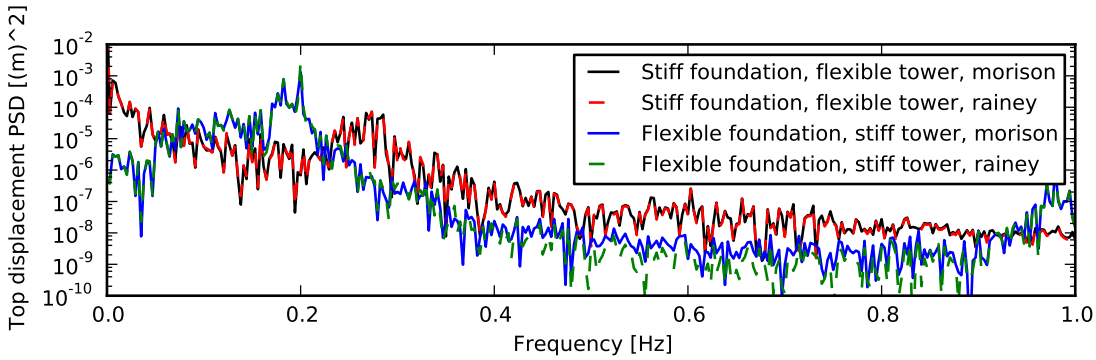

(b) PSD, parked turbine

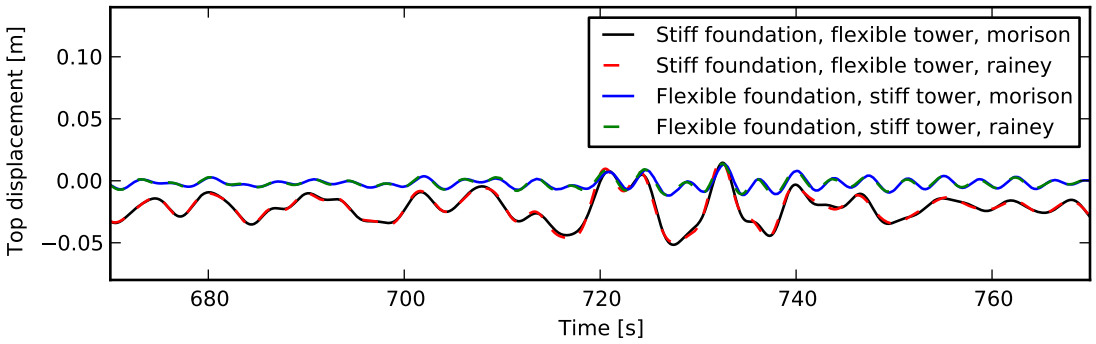

(c) Time series, no wind

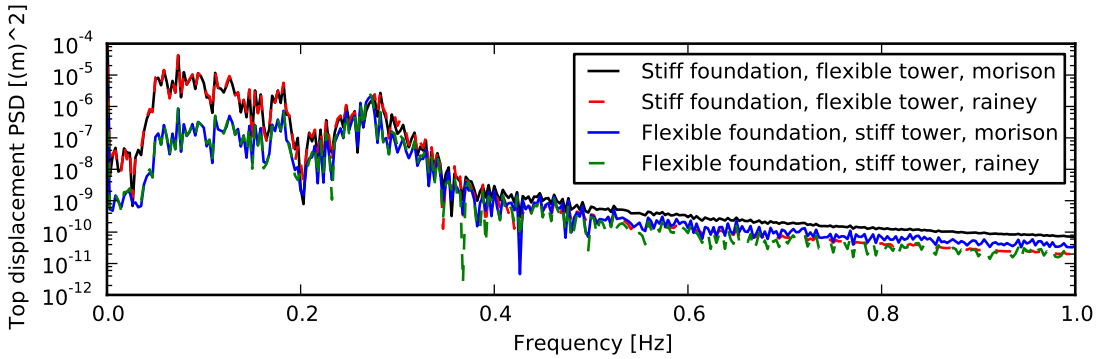

(d) PSD, no wind

Figure 4.15: *Comparison between two different configurations.*

4.6 Flexible Foundation, Flexible Tower

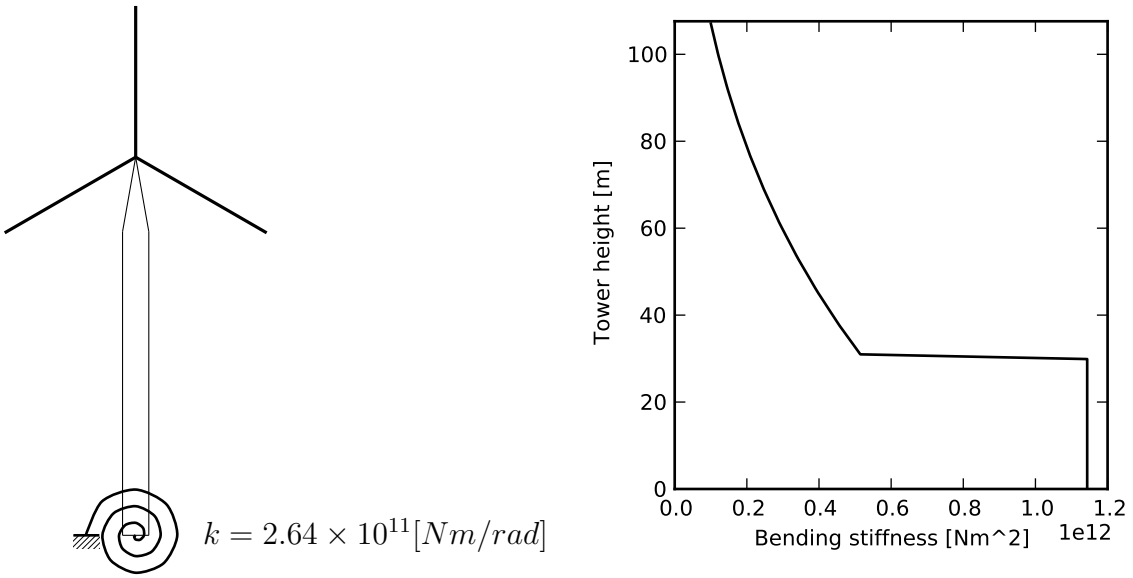

(a) Foundation stiffness.

(b) Varying stiffness along the tower.

Figure 4.16: *Soil and tower properties for the case of a flexible foundation and a flexible tower. The first natural frequency of the wind turbine tower is* $f_1 = 0.27Hz$.

Passon (2006) released a memo describing the details of the soil-pile-interaction models used for the monopile configurations from the code comparison exercise OC3 (Jonkman and Musial, 2010), where FAST was one of the participants. Linearized soil conditions based on the p-y-method was considered, and a combination of the monopile and soil ensuring a proper participation of the soil structure interaction was sought. The tower configurations used by Passon (2006) agrees well with the configuration used in this simulation, and the memo aimed at achieving a selection of soil properties based on realistic values and typical design procedures.

The soil consists of three sand layers with different properties. A coupled springs model is established, with a stiffness matrix representation for the soil-structure interaction model. The reader is referred to Passon (2006) for the details. Fig. 4.17 visualizes the translational and rotational stiffness. k_u was found to be $2.58 \times 10^9 N/m$ and k_φ was found to be $2.64 \times 10^{11} Nm/rad$. Only the rotational stiffness effect is included for this configuration, as shown in Fig. 4.16.

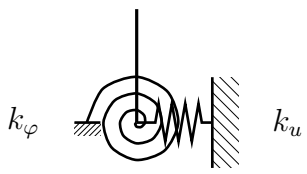

Figure 4.17: *The soil stiffness model represented by a translational and rotational stiffness at the foundation.*

Fig. 4.18 and Fig. 4.19 shows the benchmark parameters plotted in the time and frequency domain for the current configuration.

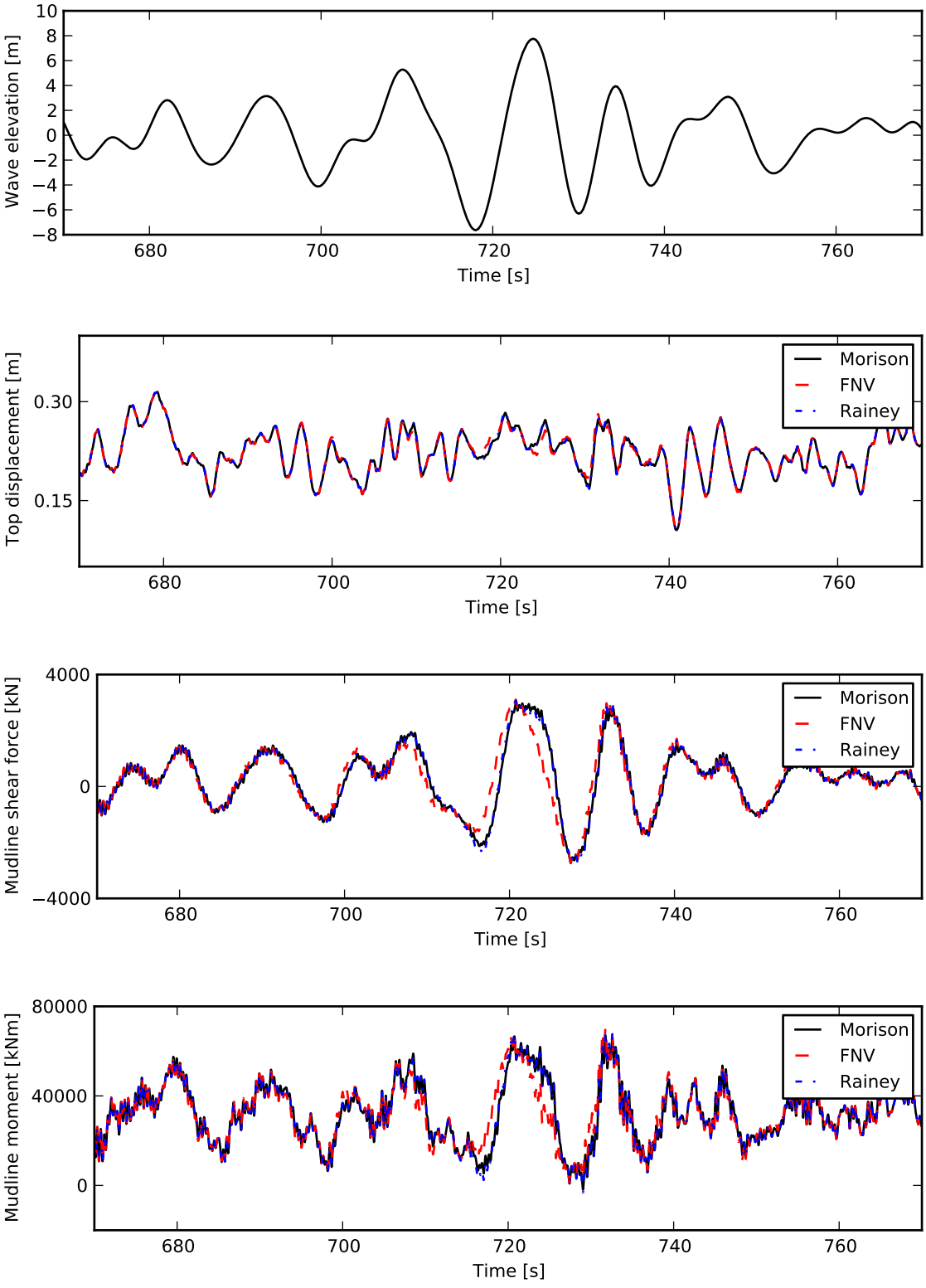

Figure 4.18: *Wave elevation, top displacement, mudline shear force and mudline moment plotted as a time series for a running turbine. A comparison is given between Morison, FNV and Rainey forces.*

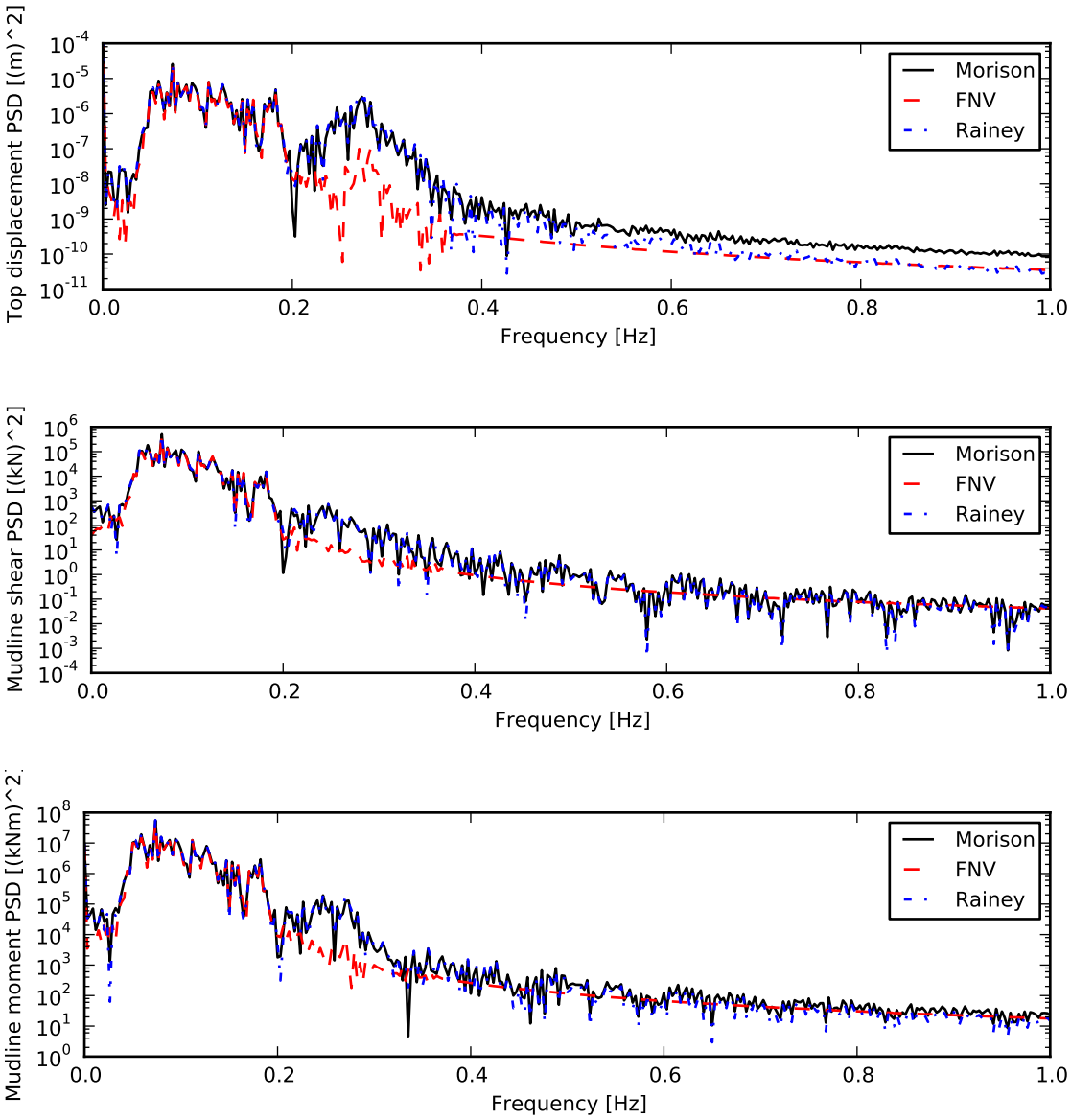

Figure 4.19: *PSD of the top displacement, mudline shear force and mudline moment for the case of no wind.*

Chapter 5

Discussion of Results, Uncertainties and Further Work

The nonlinear force models have been derived and verified using the papers where they were first presented. It was shown that for moderately high regular waves, the first and second order force components agreed, which has also been confirmed analytically by Tromans et al. (2006), building on the works by Lighthill (1979). No such analysis of the different components was conducted for irregular waves, and in fact Fig. 4.18 and 4.19 showed deviations between the FNV and Rainey forces, as discussed below.

No significant response due to nonlinear forcing was observed. No ringing event occurred. In Fig. 4.10, 4.14 and 4.19, excitations of higher frequencies than the wave frequency could not be identified, neither for the FNV or the Rainey forcing model. The largest response frequency was close to the wave excitation frequency $0.063Hz$. The top displacement of the turbine also showed a peak at the tower natural frequency $0.27Hz$. The amplitude of this response was approximately similar for the configuration with a stiff foundation and a flexible tower, and vice versa. This can bee seen from the case of no wind in Fig. 4.15, ie. only hydrodynamic loads. Thus, it seemed like the top displacement amplitude around the tower natural frequency was quite unresponsive to changing foundation and tower configurations. The response around the wave excitation frequency was higher for the case with a flexible tower.

In Fig. 4.19, it is not clear why the response due to FNV forces close to the tower natural frequency was significantly lower than the linear forces and Rainey forces. Since in the present implementation, the FNV point loads are lumped using the wave kinematics of the mean surface level, the moment will not be exact, and this may be the reason for the deviations seen in Fig. 4.19. An implementation where the point loads are distributed between the mean surface level and the free surface should be used to reveal if this is the source of error.

One of the main uncertainties of this thesis is related to the lack of model test results to compare with the implemented force models. Additionally, the lack of software for dynamic analysis of offshore wind turbines with higher order forcing capabilities according to FNV and Rainey theory, makes it difficult to assess the correctness of the implementation done in the work with this thesis. Analytical derivations of the force components as it was done in Chapter 2, or comparisons with the linear forcing as it was done in Chapter 3, are not adequate.

Some of the assumptions made when deriving the force models are not tested for the different simulation runs. The assumption of infinite water depth is certainly not

satisfied, and a survey should be carried out to see whether the force models are still valid for the applied water depth of $20m$. The evaluation of wave kinematics at the cylinder centerline instead of the cylinder wall is an assumption that is inherent in the wave models, but also the FAST software itself. This may be limiting the correctness of the integrated forces along the wind turbine tower, depending on the wave velocities and cylinder diameter.

In FAST, the tower is discretized into an evenly spaced number of elements. Future planned capabilities will include the option for arbitrary element discretization. No study was carried out to evaluate the effect of refining element sizes close to the free surface. Since the higher order FNV and Rainey components are significant near the free surface, the mesh refinement around this region could potentially be significant.

The choice of including neither wave motion or structural nonlinearities was made because these features are not supported by FAST at present, and to implement them would be demanding. It is reason to believe that nonlinear wave models would show significant contribution to the higher order forcing effects, as they are more capable than linear waves of representing realistic wave profiles of high steepness. Future work should investigate the effect of these nonlinearities.

Future work should also seek to address the influence of vertical mode shape distribution from the soil, tower and top mass on the dynamic response of the wind turbine. It was touched upon, introducing different soil and tower configurations, but no conclusion was made to this topic.

Bibliography

DNV-RP-C205 Environmental Conditions And Environmental Loads. Technical report, Det Norske Veritas, 2010.

DNV-OS-J101 Design of Offshore Wind Turbine Structures. Technical report, Det Norske Veritas, 2013.

Bir, Gunjit. NWTC design codes (BModes), 2013. URL `http://wind.nrel.gov/designcodes/preprocessors/bmodes/`.

Dean, Robert G. and Dalrymple, Robert A. *Water Wave Mechanics for Engineers and Scientist*. World Scientific, 1991.

Engebretsen, Espen André. Wave conditions for offshore wind turbine foundations in intermediate water depths. Master's thesis, Norwegian University of Science and Technology, 2012.

Faltinsen, O. M. *Sea Loads on Ships and Offshore Structures*. Cambridge University Press, 1990.

Faltinsen, O. M., Newman, J. N., and Vinje, T. Nonlinear wave loads on a slender vertical cylinder. *Journal of Fluid Mechanics*, 289:179–198, 1995.

Greco, Marilena. TMR 4215: Sea Loads - lecture notes, 2012.

Grue, John and Huseby, Morten. Higher-harmonic wave forces and ringing of vertical cylinders. *Applied Ocean Research*, 24:203–214, 2002.

Haver, Sverre K. Prediction of characteristics response for design purposes. Technical report, Statoil, 2009.

Jonkman, J. and Musial, W. Offshore code comparison collaboration (oc3) for iea task 23 offshore wind technology and deployment. Technical report, 2010.

Jonkman, J., Butterfield, S., Musial, W., and Scott, G. Definition of a 5-MW reference wind turbine for offshore system development. Technical report, National Renewable Energy Laboratory, 2009.

Jonkman, Jason. *FAST & HydroDyn*. National Renewable Energy Laboratory (NREL), 2008.

Jonkman, Jason and Buhl Jr., Marshall L. *FAST User's Guide*. National Renewable Energy Laboratory (NREL), 2005.

Jonkman, Jason and Jonkman, Bonnie. NWTC computer-aided engineering tools (FAST), 2013. URL `http://wind.nrel.gov/designcodes/simulators/fast/alpha/`.

Kreyszig, Erwin. *Advanced Engineering Mathematics*. John Wiley and Sons, 9th edition, 2006.

Krokstad, Jørgen. Private conversation, 2014.

Malenica, S. and Molin, B. Third-harmonic wave diffraction by a vertical cylinder. *J. Fluid Mech.*, 302:203–229, 1995.

Manners, W. and Rainey, R. C. T. Hydrodynamic forces on fixed submerged cylinders. *Proc. R. Soc. Lond. A*, 436:13–32, 1992.

Morison, J. R., O'Brien, M. P., Johnson, J. W., and Schaaf, S. A. The force exerted by surface waves on piles. *Journal of Petroleum Technology*, 189:149–154, 1950.

Myrhaug, Dag. Oceanography - wind, waves, 2006.

Myrhaug, Dag. Marin dynamikk - uregelmessig sjø, 2007.

Newman, J. N. *Marine Hydrodynamics*. The MIT Press, 1977.

Newman, J. N. Nonlinear scattering of long waves by a vertical cylinder. *Waves and Nonlinear Processes in Hydrodynamics*, pages 91–102, 1996.

Newman, J. N. and Lee, C.-H. Runup on a vertical cylinder in long waves. *10th Workshop on Water Waves and Floating Bodies*, pages 187–191, 1995.

Olsen, Trine Jelstad. Ikkelineær bølgeanalyse av bunnfast slank sylinder. Master's thesis, University of Oslo, 2010.

Passon, Patrik. Derivation and description of the soil-pile-interaction models. Technical report, 2006.

Press, W., Teukolsky, S., Vetterline, W. T., and Flannery, B. P. *Numerical Recipies: The Art of Scientific Computing*. Cambridge Univ. Press, 2007.

Rainey, R. C. T. A new equation for calculating wave loads on offshore structures. *J. Fluid Mech.*, 204:295–324, 1989.

Rainey, R. C. T. Slender-body expressions for the wave loads on offshore structures. *Proc. R. Soc. Lond. A*, 450:391–416, 1995.

Rosenlund, Even. Nonlinear hydrodynamic effects for bottom-fixed wind turbines. Master's thesis, Norwegian University of Science and Technology, 2013.

Tromans, Peter, Swan, Chris, and Masterton, Stephen. Nonlinear potential flow forcing: the ringing of concrete gravity based structures. Technical Report 468, Health and Safety Executive, 2006.

van der Tempel, Jan and Molenaar, David-Pieter. Wind turbine structural dynamics - a review of the principles for modern power generation, onshore and offshore. *Wind Engineering*, 26(4):211–220, 2002.

Wheeler, J. D. Method for calculating forces produced by irregular waves. *Journal of Petroleum Technology*, 22:359–367, 1970.

Appendix A

FNV Source Code

```
1  SUBROUTINE UserTwrLd ( JNode, TwrDiam, TwrCA, TwrCD, X, XD, ZTime, TwrAM, TwrFt )
2
3  ! This routine assumes that the tower loads are transmitted through a medium
4  !   like soil [foundation] and/or water [offshore], so that added mass
5  !   effects are important. Consequently, the routine assumes that the total
6  !   load per unit length on the current tower element can be written as:
7  !
8  ! TwrF(i) = SUM( -TwrAM(i,j)*XDD(j), j=1,2,..,6) + TwrFt(i) for i=1,2,...,6
9  !
10 ! where,
11 !   TwrF(i)   = the i'th component of the total load per unit length
12 !              applied on the current tower element; positive in the
13 !              direction of positive motion of the i'th DOF of the current
14 !              tower element
15 !   TwrAM(i,j) = the (i,j) component of the tower added mass matrix per unit
16 !              length (output by this routine)
17 !   XDD(j)    = the j'th component of the current tower element
18 !              acceleration vector
19 !   TwrFt(i)  = the i'th component of the portion of the current tower
20 !              element load per unit length associated with everything but
21 !              the added mass effects; positive in the direction of
22 !              positive motion of the i'th DOF of the current tower
23 !              element (output by this routine)
24
25 ! The order of indices in all arrays passed to and from this routine is as
26 !   follows:
27 !      1 = Current tower element surge / xi-component of translation
28 !      3 = Current tower element sway / yi-component of translation
29 !      3 = Current tower element heave / zi-component of translation
30 !      4 = Current tower element roll / xi-component of rotation
31 !      5 = Current tower element pitch / yi-component of rotation
32 !      6 = Current tower element yaw / zi-component of rotation
33
34 ! NOTE: The added mass matrix returned by this routine, TwrAM, must be
35 !       symmetric. FAST and ADAMS will abort otherwise.
36 !
37 !       Please also note that the hydrostatic restoring contribution to the
38 !       hydrodynamic force returned by this routine should not contain the
39 !       effects of body weight, as is often done in classical marine
40 !       hydrodynamics. The effects of body weight are included within FAST
41 !       and ADAMS.
42
```

```
43 USE                          Precision
44 USE                          Waves
45
46 IMPLICIT                     NONE
47
48    ! Passed Variables:
49
50 REAL(ReKi), INTENT(OUT)    :: TwrAM (6,6) ! Added mass matrix per unit length of
       current tower element (kg/m, kg-m/m, kg-m^2/m)
51 REAL(ReKi), INTENT(IN )    :: TwrCA ! Normalized hydrodynamic added mass coefficient
        of current tower element (-)
52 REAL(ReKi), INTENT(IN )    :: TwrCD ! Normalized hydrodynamic viscous drag
       coefficient of current tower element (-)
53 REAL(ReKi), INTENT(IN )    :: TwrDiam ! Diameter of current tower element (meters)
54 REAL(ReKi), INTENT(OUT)    :: TwrFt   (6) ! The surge/xi (1), sway/yi (2), and heave
       /zi (3)-components of the portion of the tower force per unit length (in N/m)
       at the current tower element and the roll/xi (4), pitch/yi (5), and yaw/zi (6)-
       components of the portion of the tower moment per unit length (in N-m/m) acting
        at the current tower element associated with everything but the added-mass
       effects; positive forces are in the direction of motion.
55 REAL(ReKi), INTENT(IN )    :: X       (6) ! The 3 components of the translational
       displacement (in m ) of the current tower node and the 3 components of the
       rotational displacement (in rad ) of the current tower element relative to the
       inertial frame origin at ground level [onshore] or MSL [offshore].
56 REAL(ReKi), INTENT(IN )    :: XD      (6) ! The 3 components of the translational
       velocity (in m/s) of the current tower node and the 3 components of the
       rotational (angular) velocity (in rad/s) of the current tower element relative
       to the inertial frame origin at ground level [onshore] or MSL [offshore].
57 REAL(ReKi), INTENT(IN )    :: ZTime ! Current simulation time (sec)
58
59 INTEGER(4), INTENT(IN )    :: JNode ! The number of the current tower node / element
        (-) [1 to TwrNodes]
60
61    ! Local Variables:
62
63 REAL(ReKi)                  :: DZFract ! The fraction of the current tower element
       that is below the free surface of the incident wave and above the seabed (0.0
       <= DZFract <= 1.0): 0.0 = the element is entirely above the free surface, 1.0 =
        element is entirely below the free surface and above the seabed (-)
64 REAL(ReKi)                  :: DZFractS ! The fraction of the current tower element
       that is above the seabed (0.0 <= DZFractS <= 1.0): 0.0 = the element is
       entirely below the seabed, 1.0 = element is entirely above the seabed (-)
65 REAL(ReKi)                  :: DZFractW                                    ! The
       fraction of the current tower element that is below the free surface of the
       incident wave (0.0 <= DZFractW <= 1.0): 0.0 = the element is entirely above the
        free surface, 1.0 = element is entirely below the free surface (-)
66 REAL(ReKi)                  :: InertiaForce(2) ! Wave inertia force in the xi- (1)
       and yi- (2) directions, respectively, on the current tower element at the
       current time (N)
67 REAL(ReKi)                  :: MagVRel ! The magnitude of the horizontal incident
       wave velocity relative to the current tower node at the current time (m/s)
68 REAL(ReKi)                  :: MomArm ! Moment arm in the vertical direction from the
        current tower node to the center of pressure of the wave load on the current
       tower element (meters)
69 REAL(ReKi)                  :: TowerAM ! Force -translation component of TwrAM (kg /m
       )
70 REAL(ReKi)                  :: TowerAMM ! Force -rotation and moment-translation
```

```
      component of TwrAM (kg-m /m)
71 REAL(ReKi)                 :: TowerAMM2 ! Moment-rotation component of TwrAM (kg-m
      ^2/m)
72 REAL(ReKi)                 :: TwrArea ! Cross-sectional area of current tower
      element (m^2)
73 REAL(ReKi)                 :: TwrVelocity(2) ! Velocity of the center of pressure of
       the wave load on the current tower element in the xi- (1) and yi- (2)
      directions, respectively, at the current time (m/s)
74 REAL(ReKi)                 :: ViscousForce(2) ! Viscous drag force in the xi- (1)
      and yi- (2) directions, respectively, on the current tower element at the
      current time (N)
75 REAL(ReKi)                 :: WaveAcceleration0(3) ! Acceleration of incident waves
      in the xi- (1) and yi- (2) directions, respectively, at the current tower node
      and time (m/s^2)
76 REAL(ReKi)                 :: WaveElevation0 ! Elevation of incident waves at the
      platform reference point and current time (meters)
77 REAL(ReKi)                 :: WaveVelocity0(3) ! Velocity  of incident waves in the
      xi- (1) and yi- (2) directions, respectively, at the current tower node and
      time (m/s )
78 REAL(ReKi)                 :: WaveVelocityGradient0(3,3) ! Wave velocity gradient
      matrix
79 REAL(ReKi)                 :: WaveVelocitySurf0(3) ! Wave velocity vector at surface
       intersection
80 REAL(ReKi)                 :: WaveAccelerationSurf0(3) ! Wave acceleration vector at
       surface intersection
81 REAL(ReKi)                 :: WavedudzSurface0(3)
82 REAL(ReKi)                 :: Waved2udtdzSurface0(3)
83 REAL(ReKi)                 :: FNV(2) ! Total FNV force in x- and y-direction
84 REAL(ReKi)                 :: FNV1_1(2) ! First order FNV force
85 REAL(ReKi)                 :: FNV2_1(2) ! Second order distributed FNV force
86 REAL(ReKi)                 :: FNV2_2(2) ! Second order FNV point force
87 REAL(ReKi)                 :: FNV3_1(2) ! Third order FNV force from linear
      potential
88 REAL(ReKi)                 :: FNV3_2(2) ! Third order FNV force from non-linear
      potential
89
90 INTEGER(4)                 :: K ! Generic index
91
92    ! Initialize the added mass matrix per unit length of the current tower
93    !   element, TwrAM, and the portion of the current tower element load per
94    !   unit length associated with everything but the added mass effects,
95    !   TwrFt, to zero:
96
97 TwrAM(1,:) = (/ 0.0, 0.0, 0.0, 0.0, 0.0, 0.0 /)
98 TwrAM(2,:) = (/ 0.0, 0.0, 0.0, 0.0, 0.0, 0.0 /)
99 TwrAM(3,:) = (/ 0.0, 0.0, 0.0, 0.0, 0.0, 0.0 /)
100 TwrAM(4,:) = (/ 0.0, 0.0, 0.0, 0.0, 0.0, 0.0 /)
101 TwrAM(5,:) = (/ 0.0, 0.0, 0.0, 0.0, 0.0, 0.0 /)
102 TwrAM(6,:) = (/ 0.0, 0.0, 0.0, 0.0, 0.0, 0.0 /)
103
104 TwrFt(1)  = 0.0
105 TwrFt(2)  = 0.0
106 TwrFt(3)  = 0.0
107 TwrFt(4)  = 0.0
108 TwrFt(5)  = 0.0
109 TwrFt(6)  = 0.0
110
```

```
111    ! Find the fraction of the current tower element that is below the free
112    !   surface of the incident wave and above the seabed:
113
114 IF ( WaveStMod == 0 ) THEN ! .TRUE. if we have no stretching; therefore, integrate
       up to the MSL, regardless of the instantaneous free surface elevation.
115
116    IF (     ( WaveKinzi0(JNode) - 0.5*DZNodes(JNode) ) >= 0.0      ) THEN ! .TRUE.
           if the current tower element lies entirely above the MSL.
117       DZFractW = 0.0
118    ELSEIF ( ( WaveKinzi0(JNode) + 0.5*DZNodes(JNode) ) <= 0.0      ) THEN ! .TRUE.
           if the current tower element lies entirely below the MSL.
119       DZFractW = 1.0
120    ELSE                                                                 ! The free
           surface of the incident wave must fall somewhere along the current tower
           element; thus, interpolate.
121       DZFractW = ( ( 0.0          - ( WaveKinzi0(JNode) - 0.5*DZNodes(JNode) ) )/
              DZNodes(JNode) )
122    ENDIF
123
124 ELSE                          ! We must have some sort of stretching.
125
126    WaveElevation0 = WaveElevation ( 1, ZTime )
127
128    IF (     ( WaveKinzi0(JNode) - 0.5*DZNodes(JNode) ) >= WaveElevation0 ) THEN ! .
           TRUE. if the current tower element lies entirely above the free surface of
           the incident wave.
129       DZFractW = 0.0
130    ELSEIF ( ( WaveKinzi0(JNode) + 0.5*DZNodes(JNode) ) <= WaveElevation0 ) THEN ! .
           TRUE. if the current tower element lies entirely below the free surface of
           the incident wave.
131       DZFractW = 1.0
132    ELSE                                                                 ! The free
           surface of the incident wave must fall somewhere along the current tower
           element; thus, interpolate.
133       DZFractW = ( ( WaveElevation0 - ( WaveKinzi0(JNode) - 0.5*DZNodes(JNode) ) )/
              DZNodes(JNode) )
134    ENDIF
135
136 ENDIF
137
138 IF (       ( WaveKinzi0(JNode) - 0.5*DZNodes(JNode) ) >= -WtrDpth )  THEN ! .TRUE.
       if the current tower element lies entirely above the seabed.
139       DZFractS = 1.0
140 ELSEIF (   ( WaveKinzi0(JNode) + 0.5*DZNodes(JNode) ) <= -WtrDpth )  THEN ! .TRUE.
       if the current tower element lies entirely below the seabed.
141       DZFractS = 0.0
142 ELSE                                                                 ! The
       seabed must fall somewhere along the current tower element; thus, interpolate.
143       DZFractS = ( ( ( WaveKinzi0(JNode) + 0.5*DZNodes(JNode) ) - ( -WtrDpth ) )/
              DZNodes(JNode) )
144 ENDIF
145
146 DZFract = DZFractW*DZFractS
147
148    ! Compute the hydrodynamic loads using FNV equations for the portion of
149    !   the current tower element that lies below the free surface of the
150    !   incident wave and above the seabed:
```

```
151
152 IF ( DZFract > 0.0 ) THEN ! .TRUE. if a portion of the current tower element lies
      below the free surface of the incident wave.
153
154    ! Compute the moment arm in the vertical direction between the current tower
155    !   node and the center of pressure of the wave load on the current tower
156    !   element:
157
158    MomArm = 0.5*DZNodes(JNode)*( DZFractW - DZFractS ) ! NOTE: MomArm = 0.0 when
          the entire element is submerged in the fluid; consequently, the roll and
          pitch components of the load are zero when the entire element is submerged
          in the fluid
159
160    ! Compute the velocity and acceleration of the incident waves in the xi- (1)
161    !   and yi- (2) directions, respectively, at the current tower node and
162    !   time:
163
164    DO K = 1,3    ! Loop through the xi- (1) and yi- (2) directions
165       WaveVelocity0  (K) = WaveVelocity   ( JNode, K, ZTime )
166       WaveAcceleration0(K) = WaveAcceleration ( JNode, K, ZTime )
167       WaveVelocityGradient0 (1,K) = WaveVelocityGradient(JNode, K, ZTime)
168       WaveVelocityGradient0 (2,K) = WaveVelocityGradient(JNode, K+3, ZTime)
169       WaveVelocityGradient0 (3,K) = WaveVelocityGradient(JNode, K+6, ZTime)
170    ENDDO         ! K - The xi- (1) and yi- (2) directions
171
172    ! Compute the velocity of the center of pressure of the wave load on the
173    !   current tower element in the xi- (1) and yi- (2) directions,
174    !   respectively, at the current time:
175
176    TwrVelocity(1) = XD(1) + XD(5)*MomArm
177    TwrVelocity(2) = XD(2) - XD(4)*MomArm
178
179    ! Compute the magnitude of the horizontal incident wave velocity relative to
180    !   the center of pressure of the wave load on the current tower element at
181    !   the current time:
182
183    MagVRel = SQRT( ( WaveVelocity0(1) - TwrVelocity(1) )**2 &
184                  + ( WaveVelocity0(2) - TwrVelocity(2) )**2 )
185
186    ! Compute the cross-sectional area of the current tower element:
187
188    TwrArea = PiOvr4*TwrDiam*TwrDiam
189
190    ! Compute the added mass matrix per unit length of the current tower
191    !   element:
192
193    TowerAM   = TwrCA*WtrDens*TwrArea*DZFract ! force -translation
          component
194    TowerAMM  = TowerAM *MomArm               ! force -rotation and moment-translation
          component
195    TowerAMM2 = TowerAMM*MomArm               !                   moment-rotation
          component
196
197    TwrAM(1,1) = TwrAM(1,1) + TowerAM ! surge-surge component
198    TwrAM(2,2) = TwrAM(2,2) + TowerAM ! sway -sway component
199    TwrAM(4,4) = TwrAM(4,4) + TowerAMM2 ! roll -roll component
200    TwrAM(5,5) = TwrAM(5,5) + TowerAMM2 ! pitch-pitch component
```

```
201   TwrAM(2,4) = TwrAM(2,4) - TowerAMM ! sway -roll component
202   TwrAM(4,2) = TwrAM(4,2) - TowerAMM ! roll -sway component
203   TwrAM(1,5) = TwrAM(1,5) + TowerAMM ! surge-pitch component
204   TwrAM(5,1) = TwrAM(5,1) + TowerAMM ! pitch-surge component
205
206   ! Compute the wave velocity and acceleration at surface intersection
207
208   WaveVelocitySurf0(1) = WaveVelocitySurface(1, ZTime)
209   WaveVelocitySurf0(2) = WaveVelocitySurface(2, ZTime)
210   WaveVelocitySurf0(3) = WaveVelocitySurface(3, ZTime)
211
212   WaveAccelerationSurf0(1) = WaveAccelerationSurface(1, ZTime)
213   WaveAccelerationSurf0(2) = WaveAccelerationSurface(2, ZTime)
214   WaveAccelerationSurf0(3) = WaveAccelerationSurface(3, ZTime)
215
216   WavedudzSurface0(1) = WavedudzSurface(1, ZTime)
217   WavedudzSurface0(2) = WavedudzSurface(2, ZTime)
218   WavedudzSurface0(3) = WavedudzSurface(3, ZTime)
219
220   Waved2udtdzSurface0(1) = Waved2udtdzSurface(1, ZTime)
221   Waved2udtdzSurface0(2) = Waved2udtdzSurface(2, ZTime)
222   Waved2udtdzSurface0(3) = Waved2udtdzSurface(3, ZTime)
223
224   ! Compute the portions of the current tower element load per unit length
225   !   associated with the incident wave acceleration and the viscous drag:
226
227   DO K = 1,2    ! Loop through the xi- (1) and yi- (2) directions
228
229      ! Compute the distributed FNV load components
230      FNV1_1(K) = ( 1.0 + TwrCA )*WtrDens*TwrArea*WaveAcceleration0(K)*DZFract
231      FNV2_2(K) = WtrDens*TwrArea*WaveVelocity0(3)*WaveVelocityGradient0(K,3)*
             DZFract
232
233      ! Compute the viscous forces
234      ViscousForce(K) = 0.5*TwrCD*WtrDens*TwrDiam*( WaveVelocity0(K) - TwrVelocity(K
             ) )*MagVRel*DZFract
235
236      ! Calculate the FNV point loads at surface intersections
237      IF ( DZFractW < 1.0 .AND. DZFractW > 0.0 ) THEN
238
239         FNV2_1(K) = 2 * WtrDens * TwrArea * WaveAccelerationSurf0(K) *
                 WaveElevation0 / DZNodes(JNode)
240         FNV3_1(K) = WtrDens * TwrArea * WaveElevation0 * (Waved2udtdzSurface0(K) *
                 WaveElevation0 + WaveVelocitySurf0(3) * WavedudzSurface0(K) - 2 / 9.81
                 * WaveAccelerationSurf0(K) * WaveAccelerationSurf0(3)) / DZNodes(JNode)
241         FNV3_2(K) = 4 / 9.81 * WtrDens * TwrArea * WaveVelocitySurf0(K) *
                 WaveVelocitySurf0(K) * WaveAccelerationSurf0(K) / DZNodes(JNode)
242
243      ELSE
244
245         FNV2_1(K) = 0.0
246         FNV3_1(K) = 0.0
247         FNV3_2(K) = 0.0
248
249      ENDIF
250
251   ENDDO         ! K - The xi- (1) and yi- (2) directions
```

```
252
253    TwrFt(1 ) = TwrFt(1 ) +  FNV1_1(1) + FNV2_1(1) + FNV2_2(1) + FNV3_1(1) + FNV3_2
           (1) + ViscousForce(1)   ! surge component
254    TwrFt(2 ) = TwrFt(2 ) +  FNV1_1(2) + FNV2_1(2) + FNV2_2(2) + FNV3_1(2) + FNV3_2
           (2) + ViscousForce(2)   ! sway component
255    TwrFt(4 ) = TwrFt(4 ) - ( FNV1_1(2) + FNV2_2(2) + ViscousForce(2) )*MomArm -
           0.5*(FNV2_1(2)+FNV3_1(2)+FNV3_2(2))*(WaveElevation0 - WaveKinzi0(JNode)) !
           roll component
256    TwrFt(5 ) = TwrFt(5 ) + ( FNV1_1(1) + FNV2_2(1) + ViscousForce(1) )*MomArm +
           0.5*(FNV2_1(1)+FNV3_1(1)+FNV3_2(1))*(WaveElevation0 - WaveKinzi0(JNode)) !
           pitch component
257
258 ENDIF
259
260 RETURN
261 END SUBROUTINE UserTwrLd
```

Appendix B

Rainey Source Code

```
1 SUBROUTINE UserTwrLd ( JNode, TwrDiam, TwrCA, TwrCD, X, XD, ZTime, TwrAM, TwrFt )
2
3 ! <--- Same declaration and initialization as for the FNV source code. --->
4
5    ! Compute the hydrodynamic loads using Rainey equations for the portion of
6    !   the current tower element that lies below the free surface of the
7    !   incident wave and above the seabed:
8
9 IF ( DZFract > 0.0 ) THEN ! .TRUE. if a portion of the current tower element lies
      below the free surface of the incident wave.
10
11
12   ! Compute the moment arm in the vertical direction between the current tower
13   !   node and the center of pressure of the wave load on the current tower
14   !   element:
15
16   MomArm = 0.5*DZNodes(JNode)*( DZFractW - DZFractS ) ! NOTE: MomArm = 0.0 when
         the entire element is submerged in the fluid; consequently, the roll and
         pitch components of the load are zero when the entire element is submerged
         in the fluid
17
18
19   ! Compute the velocity and acceleration of the incident waves in the xi- (1)
20   !   and yi- (2) directions, respectively, at the current tower node and
21   !   time:
22
23   DO K = 1,3    ! Loop through the xi- (1) and yi- (2) and zi- (3) directions
24      WaveVelocity0  (K) = WaveVelocity   ( JNode, K, ZTime )
25      WaveAcceleration0(K) = WaveAcceleration ( JNode, K, ZTime )
26      WaveVelocityGradient0 (1,K) = WaveVelocityGradient(JNode, K, ZTime)
27      WaveVelocityGradient0 (2,K) = WaveVelocityGradient(JNode, K+3, ZTime)
28      WaveVelocityGradient0 (3,K) = WaveVelocityGradient(JNode, K+6, ZTime)
29   ENDDO         ! K - The xi- (1) and yi- (2) and zi- (3) directions
30
31   ! Calculate the convective accelerations
32
33   WaveConvAcc0(1) = WaveVelocity0(1)*WaveVelocityGradient0(1,1) + WaveVelocity0(2)
         *WaveVelocityGradient0(1,2) + WaveVelocity0(3)*WaveVelocityGradient0(1,3)
34   WaveConvAcc0(2) = WaveVelocity0(1)*WaveVelocityGradient0(2,1) + WaveVelocity0(2)
         *WaveVelocityGradient0(2,2) + WaveVelocity0(3)*WaveVelocityGradient0(2,3)
35   WaveConvAcc0(3) = WaveVelocity0(1)*WaveVelocityGradient0(3,1) + WaveVelocity0(2)
         *WaveVelocityGradient0(3,2) + WaveVelocity0(3)*WaveVelocityGradient0(3,3)
```

```
36
37
38    ! Compute the velocity of the center of pressure of the wave load on the
39    !   current tower element in the xi- (1) and yi- (2) directions,
40    !   respectively, at the current time:
41
42    TwrVelocity(1) = XD(1) + XD(5)*MomArm
43    TwrVelocity(2) = XD(2) - XD(4)*MomArm
44    TwrVelocity(3) = XD(4)*MomArm - XD(5)*MomArm
45
46
47    ! Compute the magnitude of the horizontal incident wave velocity relative to
48    !   the center of pressure of the wave load on the current tower element at
49    !   the current time:
50
51    MagVRel = SQRT( ( WaveVelocity0(1) - TwrVelocity(1) )**2 &
52                  + ( WaveVelocity0(2) - TwrVelocity(2) )**2 )
53
54
55    ! Compute the cross-sectional area of the current tower element:
56
57    TwrArea = PiOvr4*TwrDiam*TwrDiam
58
59
60    ! Compute the added mass matrix per unit length of the current tower
61    !   element:
62
63    TowerAM   = TwrCA*WtrDens*TwrArea*DZFract ! force -translation
          component
64    TowerAMM  = TowerAM *MomArm               ! force -rotation and moment-translation
           component
65    TowerAMM2 = TowerAMM*MomArm               !                   moment-rotation
          component
66
67    TwrAM(1,1) = TwrAM(1,1) + TowerAM ! surge-surge component
68    TwrAM(2,2) = TwrAM(2,2) + TowerAM ! sway -sway component
69    TwrAM(4,4) = TwrAM(4,4) + TowerAMM2 ! roll -roll component
70    TwrAM(5,5) = TwrAM(5,5) + TowerAMM2 ! pitch-pitch component
71    TwrAM(2,4) = TwrAM(2,4) - TowerAMM ! sway -roll component
72    TwrAM(4,2) = TwrAM(4,2) - TowerAMM ! roll -sway component
73    TwrAM(1,5) = TwrAM(1,5) + TowerAMM ! surge-pitch component
74    TwrAM(5,1) = TwrAM(5,1) + TowerAMM ! pitch-surge component
75
76
77    ! Calculate the two dimensional added mass matrix
78
79    TwoDimAM(1,1) = TwrCA*WtrDens*TwrArea
80    TwoDimAM(2,2) = TwrCA*WtrDens*TwrArea
81
82    ! Calculate the wave slope at surface
83    WaveSlopeSurf0(1) = WaveSlope(ZTime)*abs(CWavedir)
84    WaveSlopeSurf0(2) = WaveSlope(ZTime)*abs(SWavedir)
85    WaveSlopeSurf0(3) = 0.0
86
87    ! Calculate wave velocity at surface
88    WaveVelocitySurf0(1) = WaveVelocitySurface(1, ZTime)
89    WaveVelocitySurf0(2) = WaveVelocitySurface(2, ZTime)
```

```
90    WaveVelocitySurf0(3) = WaveVelocitySurface(3, ZTime)
91
92
93    ! Compute the portions of the current tower element load per unit length
94    !   associated with the incident wave acceleration and the viscous drag:
95
96    DO K = 1,2    ! Loop through the xi- (1) and yi- (2) directions
97
98       InertiaForce(K) = ( 1.0 + TwrCA ) * WtrDens * TwrArea * (WaveAcceleration0(K)
             + WaveConvAcc0(K)) * DZFract
99       AxialDivForce(K) = WtrDens * TwrArea * WaveVelocity0(K) *
             WaveVelocityGradient0(3,3) * DZFract
100      ViscousForce(K) = 0.5 * TwrCD * WtrDens * TwrDiam * ( WaveVelocity0(K) -
             TwrVelocity(K) ) * MagVRel * DZFract
101
102
103      ! Calculate the point loads at surface intersections
104
105      IF ( DZFractW < 1.0 .AND. DZFractW > 0.0 ) THEN
106
107         PointLoad(K) = -0.5 * WaveSlopeSurf0(K) * WtrDens * TwrArea *
               WaveVelocitySurf0(K)**2 / DZNodes(JNode)
108
109      ELSE
110
111         PointLoad(K) = 0.0
112
113      ENDIF
114
115
116   ENDDO         ! K - The xi- (1) and yi- (2) directions
117
118   ! Calculate the tower loads
119
120   TwrFt(1 ) = TwrFt(1 ) +  InertiaForce(1) + AxialDivForce(1) + ViscousForce(1) +
          PointLoad(1)    ! surge component
121   TwrFt(2 ) = TwrFt(2 ) +  InertiaForce(2) + AxialDivForce(2) + ViscousForce(2) +
          PointLoad(2)    ! sway component
122   TwrFt(4 ) = TwrFt(4 ) - ( InertiaForce(2) + AxialDivForce(2) + ViscousForce(2) )
          *MomArm - PointLoad(2)*(WaveElevation0 - WaveKinzi0(JNode)) ! roll component
123   TwrFt(5 ) = TwrFt(5 ) + ( InertiaForce(1) + AxialDivForce(1) + ViscousForce(1) )
          *MomArm + PointLoad(1)*(WaveElevation0 - WaveKinzi0(JNode)) ! pitch
          component
124
125
126 ENDIF
127
128 RETURN
129 END SUBROUTINE UserTwrLd
```